Universal rules govern plasmid copy number

Paula Ramiro-Martínez[1], Ignacio de Quinto[1], João Alves Gama[1], and Jerónimo Rodríguez-Beltrán*[,1,2]

1. Microbiology Department. Hospital Universitario Ramón y Cajal-IRYCIS, Madrid, Spain.
2. Centro de Investigación Biomédica en Red de Enfermedades Infecciosas (CIBERINFEC), Instituto de Salud Carlos III, Madrid, Spain.

* Correspondence and requests for materials should be addressed to JR-B at jeronimo.rodriguez.beltran@gmail.com

Abstract

Plasmids –autonomously replicating DNA molecules– are pervasive in the microbial world, where they fuel evolution as key vehicles for gene transfer. Plasmids are as diverse as their hosts and exhibit a broad range of replication and mobility strategies, genetic repertoires, host ranges, sizes, and copies per cell. While most of these features have been extensively characterized, the determinants of plasmid copy number (PCN) remain poorly understood. Here, we leveraged extensive DNA sequencing data to comprehensively analyze the copy number of thousands of diverse bacterial plasmids. We found that the copy number of natural plasmids is highly variable, spanning nearly three orders of magnitude, and that it is intrinsically robust against changes in genomic context. We further show that PCN variability is tightly associated with plasmid lifestyles and develop the concept of replicon dominance to explain interactions in widespread multi-replicon plasmids. Finally, we uncover a universal scaling law that links copy number and plasmid size across phylogenetic boundaries, indicating that pervasive constraints orchestrate the PCN-size trade-off. Altogether, our work pioneers large-scale analyses of PCN while uncovering the fundamental rules that govern plasmid biology.

Introduction

Plasmids are typically circular, autonomously replicating DNA molecules that stably coexist with host chromosomes. As the main drivers of horizontal gene transfer, plasmids can cross phylogenetic boundaries and be present in different microbial genera, families, and even life domains[1]. Plasmids are pervasive and show a plethora of replication and mobility strategies, lengths, host ranges, topologies, G+C contents, and genetic repertoires, including antibiotic resistance and virulence genes[2–6].

Plasmids ensure their stability in microbial populations thanks to fine-tuned replication mechanisms that maintain a given number of plasmid copies per cell. Plasmid copy number (PCN) is thus a fundamental aspect of plasmid biology that governs plasmid lifestyles. Some plasmids, for instance, lack active partition systems and rely on being present at a high PCN to stochastically guarantee their inheritance and persistence in the population[7]. On the other hand, plasmids encoding active segregation and partition systems are typically present at low PCN, likely reducing their metabolic load on the host and alleviating their fitness cost[8].

Moreover, PCN modulates plasmid evolvability. A high PCN increases the dosage and, proportionally, the expression of plasmid-encoded genes, which is advantageous under antibiotic pressure or in many other stressful environments[9,10]. In addition, variation in PCN within populations generates heterogeneity in gene expression, facilitating bacterial adaptation through phenotypic plasticity[1,11,12]. At longer timescales, copy number determines the evolution of plasmid genes by affecting key parameters such as mutation and recombination rates or genetic drift[1,13,14].

Results

Despite its paramount importance for microbial biology and evolution, PCN remains relatively understudied. Traditionally, PCN determinations have relied on burdensome experimental techniques (e.g., qPCR, Southern blot)[15] is mainly limited to well-known model plasmids (albeit with some exceptions[16]). To comprehensively understand the driving factors of PCN, we established a database of high-quality closed plasmid sequences found in bacterial genomes belonging to nine different genera of Gram-negative and Gram-positive bacteria. The selected genera comprised 95 species with biotechnological and clinical interest, such as all members of the ESKAPEE group[17] (**Figure 1**). We extracted plasmid sequences from these genomes and classified them into plasmid groups according to their replication mechanism (replicon types[18]) and similarity across whole plasmid sequence content (plasmid taxonomic units – PTUs[19], and plasmid clusters). This approach gave rise to a dataset that comprises plasmids belonging to 139 PTUs, 238 distinct replicon types, and 2,200 sequence-based clusters, indicating that it captures a significant fraction of the extant natural plasmid diversity. To estimate PCN for each of these plasmids, we calculated the trimmed mean sequencing coverage of each plasmid relative to the coverage of their host chromosome (see methods), leading to a dataset comprising 6,327 closed, circular, high-quality plasmid sequences and their respective copy numbers (**Figure 1, Extended Data Fig. 1, Supplementary Dataset 1 and Supplementary Dataset 2**).

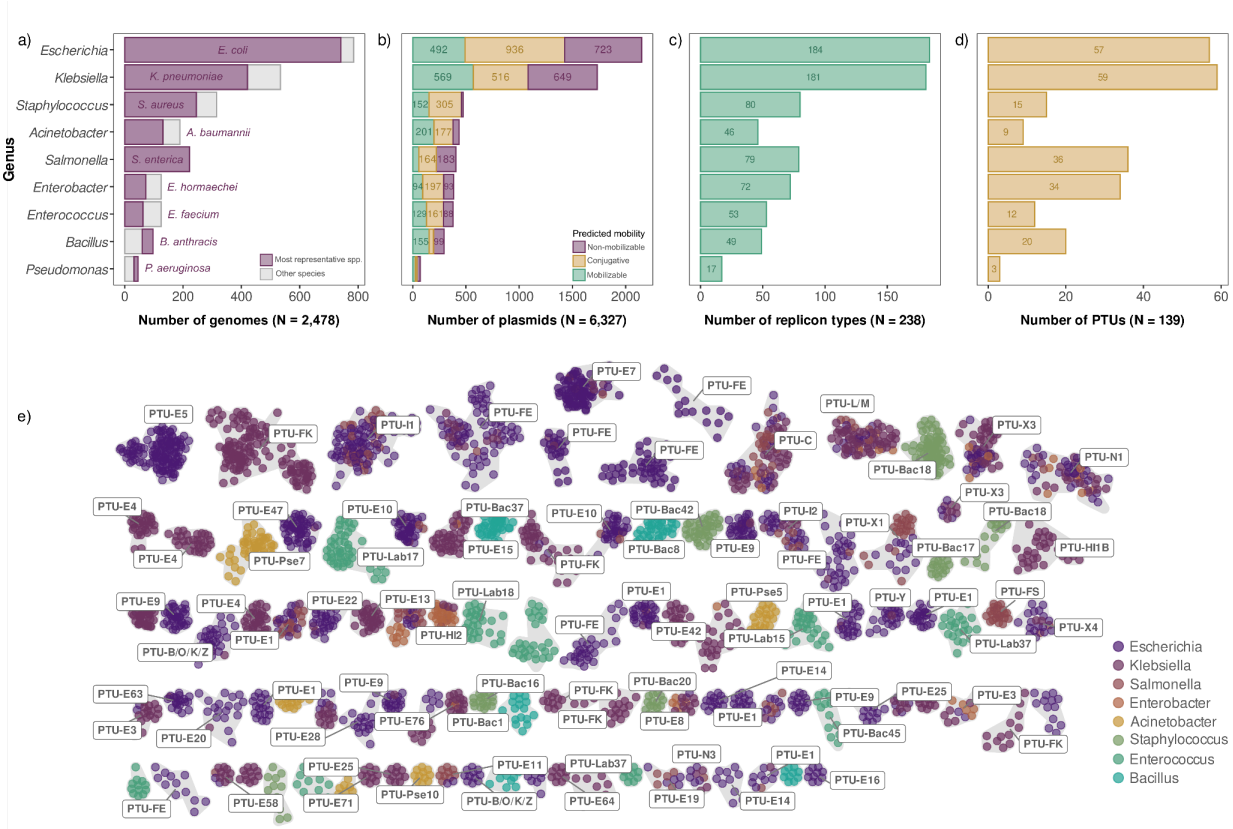

Figure 1. The plasmid dataset. a) Number of genomes (x-axis) per genus (y-axis). The most frequent species of each genus is represented in purple, while the rest are grouped and represented in grey. **b)** Number of plasmids (x-axis) per genus classified according to their predicted mobility. **c)** Number of distinct replicon types, and **d)** plasmid taxonomic units (PTUs) (x-axis) per genus. **e)** Plasmid clustering. Each node represents a plasmid, coloured according to the genus in which it was present. Clusters associated with a known PTU are indicated with a label. Clusters with less than ten plasmids are shown in **Extended Data Fig. 1**.

PCN is associated with host phylogeny, plasmid mobility, and plasmid groups

PCN was extremely variable in our dataset. PCNs displayed a broad bimodal distribution spanning three orders of magnitude (**Figure 2a**), reflecting two well-known plasmid lifestyle strategies[1,2]: Low-copy number plasmids (LCPs), typically ranging from 1 to 2 copies per chromosome (mode = 1.49) and high-copy number plasmids (HCPs), usually bearing more than ten copies per cell (mode = 10.40). Hereafter, we use the anti-mode of this distribution (i.e., the valley between both peaks: 5.75 copies) as a threshold to differentiate LCPs from HCPs. Although this threshold was largely consistent with plasmid sizes (**Extended Data Fig. 2**) and previous non-empirical definitions[7], we note that it is likely biased by the overrepresentation of Enterobacterales in our dataset and that the anti-mode in PCN distributions was not equally evident across phylogenetic levels (**Figure 2b**). Regardless of the shape of the distribution, HCPs and LCPs were present in all genera, although at different proportions: HCPs were more often found in *Escherichia* and *Enterobacter,* while *Pseudomonas*, *Enterococcus*, *Bacillus*, *Klebsiella* and *Staphylococcus* were significantly enriched in LCPs (Chi-squared test, Benjamini-Hochberg (BH) adjusted $p < 10^{-15}$, in all cases; **Figure 2c**).

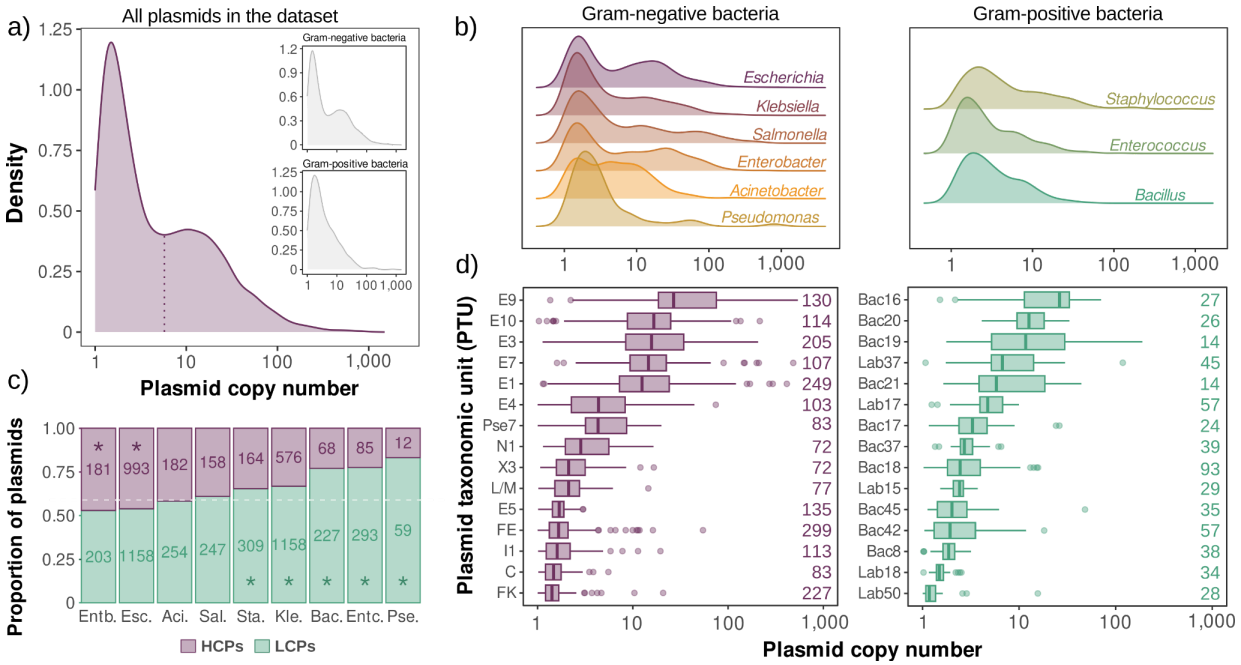

Figure 2. PCN is associated with host phylogeny and plasmid groups. a) PCN distribution for all analyzed plasmids (n=6,327). Inset plots represent the same plasmids separated according to the Gram classification of their hosts. The dotted line represents the anti-mode (5.75 copies) of the distribution. **b)** Distribution of PCN within each host genus. **c)** Proportion of HCPs (purple) and LCPs (green) (y-axis) by host genus (x-axis). The numbers within each bar denote the number of plasmids belonging to each category. Asterisks denote that the group of plasmids where they are placed (HCPs or LCPs) is significantly overrepresented compared to the complete plasmid dataset (white dashed line). The x-axis represents host genera, abbreviated to three (or four) letters. **d)** Boxplots representing the PCN per PTU from Gram-negative (purple) and -positive (green) bacteria (**Supplementary dataset 2**). Only the most abundant PTUs are indicated for each group. Numbers on the right of each boxplot show the number of plasmids belonging to each plasmid group.

Major plasmid replication types and PTUs showed a characteristic PCN (**Figure 2d, Supplementary dataset 2, Extended Data Fig. 3**). Among the most abundant plasmid groups, HCPs were mainly associated with Col-like replicons in Gram-negatives (e.g., PTUs E9, E10, E3)[20], and with rolling-circle replicating plasmids in Gram-positives (e.g., PTUs Bac20, Lab37)[21,22]. On the other hand, LCPs were frequently associated with well-characterized Gram-negative enterobacterial plasmids, such as the widespread IncF family (e.g., PTUs F_K and F_E). In Gram-positives, LCPs were diverse and included plasmids related to theta-replicating prototypical plasmids (e.g., PTU-Bac8, PTU-Bac42, PTU-Lab18)[23–26]. Regarding mobility, conjugative plasmids were typically present at low PCNs (median = 2.17), while non-mobilizable plasmids and particularly mobilizable plasmids (median = 3.94 and 8.58, respectively) were associated with a significantly higher PCN (Kruskal-Wallis test followed by Dunn's test for pairwise multiple comparisons $p < 10^{-35}$, **Extended Data Fig. 4**).

PCN is independent of the genetic repertoire, bacterial host, and co-resident plasmids

The above results highlight that each plasmid group has a characteristic PCN that is likely a direct consequence of their biology. However, there is also substantial variation in PCN within plasmid groups, at least for some of them (see, for instance, PTU-E9 and PTU-Bac19). To

characterize the sources of this variability, we first focused on how gene content and similarity affected PCN. By comparing the PCN of plasmids bearing the same replicon type but belonging to different PTUs, we found that, in general, PCN was conserved in most replicon types regardless of the genetic content (**Extended Data Fig. 5, Supplementary Dataset 3**).

Analysis of the exceptions revealed interesting plasmid biology features. For instance, Col-like plasmids from the *Escherichia*-associated PTU-E63 were present at significantly lower PCNs than those belonging to broader host range PTUs (PTU-E3 and PTU-E76) (Kruskal-Wallis test followed by Dunn's test $p < 10^{-2}$). Similarly, IncFIB/IncFII plasmids showed significant, although small, PCN differences between the *Klebsiella*-associated PTU-F_K and the *Salmonella*-associated PTU-F_S (Kruskal-Wallis test followed by Dunn's test $p < 10^{-2}$, **Extended Data Fig. 5**, **Supplementary dataset 3**).

Prompted by these observations, we next investigated the impact of host range on PCN. Of the 64 replicon types and 57 PTUs shared between at least two different genera, only 4 replicons and 5 PTUs showed significant differences in their PCN across hosts (**Extended Data Fig. 6,** see **Supplementary Dataset 4** for statistical analyses). Similarly, only two of the 13 plasmid clusters present in multiple host genera displayed significant differences in PCN between hosts (Wilcoxon rank sum test, adjusted $p < 0.04$, **Extended Data Fig. 7**). Lastly, we investigated how the presence of other plasmids within the cell affects PCN and found that only 10% of the PTUs and 7% of the replicon types showed a statistically significant correlation between PCN and the number of plasmids in the cell (Pearson's rank correlation, $p < 0.049$, n = 114 for PTUs and n = 212 for replicon types, **Supplementary Dataset 5**).

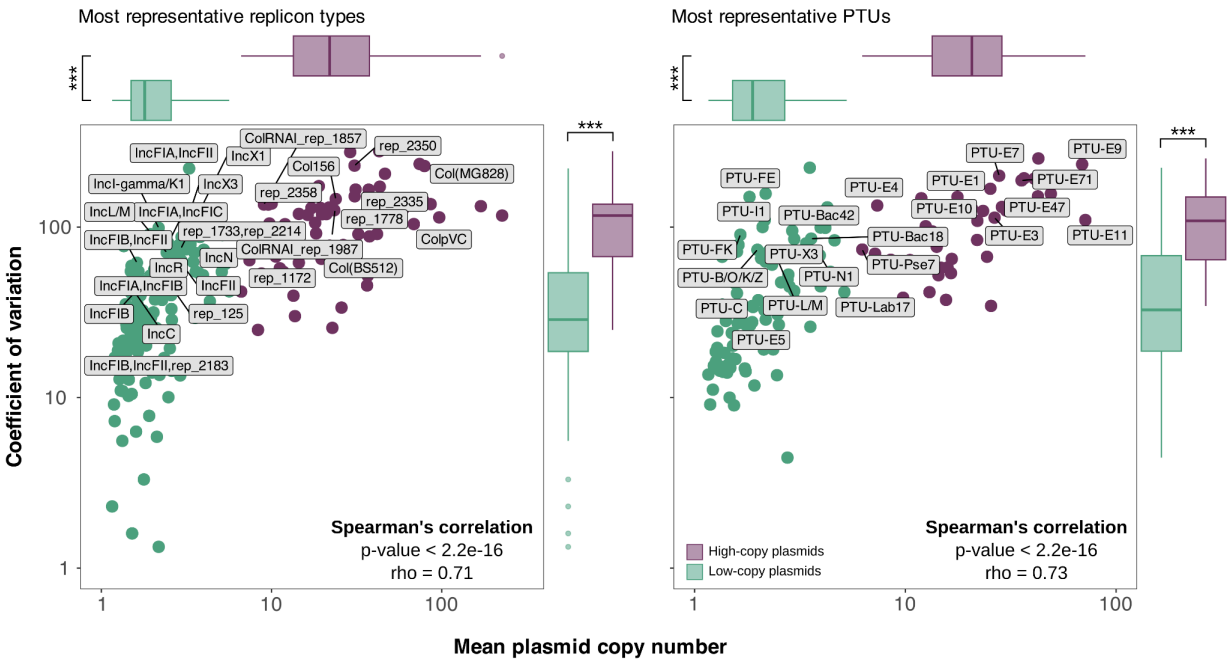

Figure 3. Intrinsic PCN variability. Correlation of PCN (x-axis) per replicon type (left) and PTU (right) with the variability in PCN as measured by the coefficient of variation (CV; y-axis). Each dot represents the mean PCN and CV for a plasmid group. The Spearman's rho and p-value for each correlation are shown at the bottom right corner of each plot. Labels indicate the most abundant plasmid groups. Colours distinguish HCP (purple) from LCP (green). Boxplots represent aggregated PCN (top) and CV (left) data for all plasmid groups, according to their classification as HCPs and LCPs. Asterisks indicate significant differences between HCPs and LCPs (***: $p < 10^{-9}$, Wilcoxon rank sum exact test).

Overall, and in agreement with previous small-scale observations[27,28], our results suggest that most plasmids encode replication control mechanisms that robustly control PCN independently of the content and identity of the plasmid's genetic repertoire, the host, and the presence of other co-resident plasmids.

Intrinsic PCN variability is higher in HCPs

We reasoned that the observed variability in PCN might be a direct manifestation of the stringency of replication control across plasmid lifestyles. In agreement with this hypothesis, HCPs showed significantly greater variability in their PCN than LCPs (measured as coefficient of variation – CV, Wilcoxon rank-sum test $p < 10^{-2}$, for both replicon types and PTUs, **Figure 3**, **Extended Data Fig. 8**). Moreover, intrinsic variability and PCN were positively and strongly correlated when we classified plasmids according to their replicon type, PTU, or plasmid cluster (Spearman's rank correlation $p < 10^{-2}$; **Figure 3**, **Extended Data Fig. 9**). As an illustrative example, the PCN of Col-like HCPs varied over two orders of magnitude (CV > 200%), while LCPs such as IncF plasmids displayed smaller variations in their PCN (CV ~ 30%; **Extended Data Fig. 10**).

In contrast to previous observations restricted to model laboratory plasmids[29,30], these results indicate that, for natural plasmids, the higher the PCN, the more relaxed the control of replication and segregation. As gene expression and PCN are tightly linked[9,10], this result underscores the role of HCPs as plastic adaptive platforms in natural settings[12]. On the other hand, biotechnological and synthetic applications may benefit from the reduced noise of LCP-derived vectors to ensure precise control of gene expression.

Replicon dominance determines plasmid copy number in multi-replicon plasmids

Multi-replicon plasmids are abundant and often occur due to plasmid co-integration, a phenomenon by which two plasmids merge as a single DNA molecule[31] (**Figure 4a**). To shed light on whether multiple replicons interact to control PCN, we tested how PCN varies for a given replicon when it drives plasmid replication alone (single replicon form) or when it coexists with other replicons within the same plasmid molecule (multi-replicon form). We found 51 replicon types present in both forms. Of those, 37% (19/51) showed significantly different PCN between the single and multi-replicon forms (Wilcoxon rank sum exact test $p < 0.047$ in all cases; **Extended Data Fig. 11**). Some replicons (e.g., IncQ1, Col156 or IncFII) exhibited a lower PCN when present in multi-replicon plasmids, while other replicons showed higher PCN (e.g., ColE1-like replicons rep_2358 and rep_2370; **Figure 4b**). This demonstrates that interactions between co-existing replicons frequently alter PCN.

To explain these interactions, we borrowed from classical genetics and conceived the concept of *replicon dominance*. We observed that in certain replicon combinations, one of the replicons did not contribute to the final number of plasmid copies (i.e., it was recessive), and the PCN was controlled by the other replicon(s) (i.e., dominant) (**Figure 4c**). Higher copy number replicons were generally recessive to replicons showing lower copy numbers (**Figure 4d, Extended data Fig. 12**). For instance, HCP-associated replicons were recessive to LCP replicons, possibly because their replication mechanism (e.g., strand displacement) is unsuitable for efficiently replicating larger plasmids (**Figure 4d, Extended Data Fig. 12**). On the other hand, plasmids containing multiple LCP-associated replicons showed variable

dominance patterns, with either the lower or the higher PCN replicon being dominant, albeit PCN differences were generally small (**Figure 4e, Extended Data Fig. 12**).

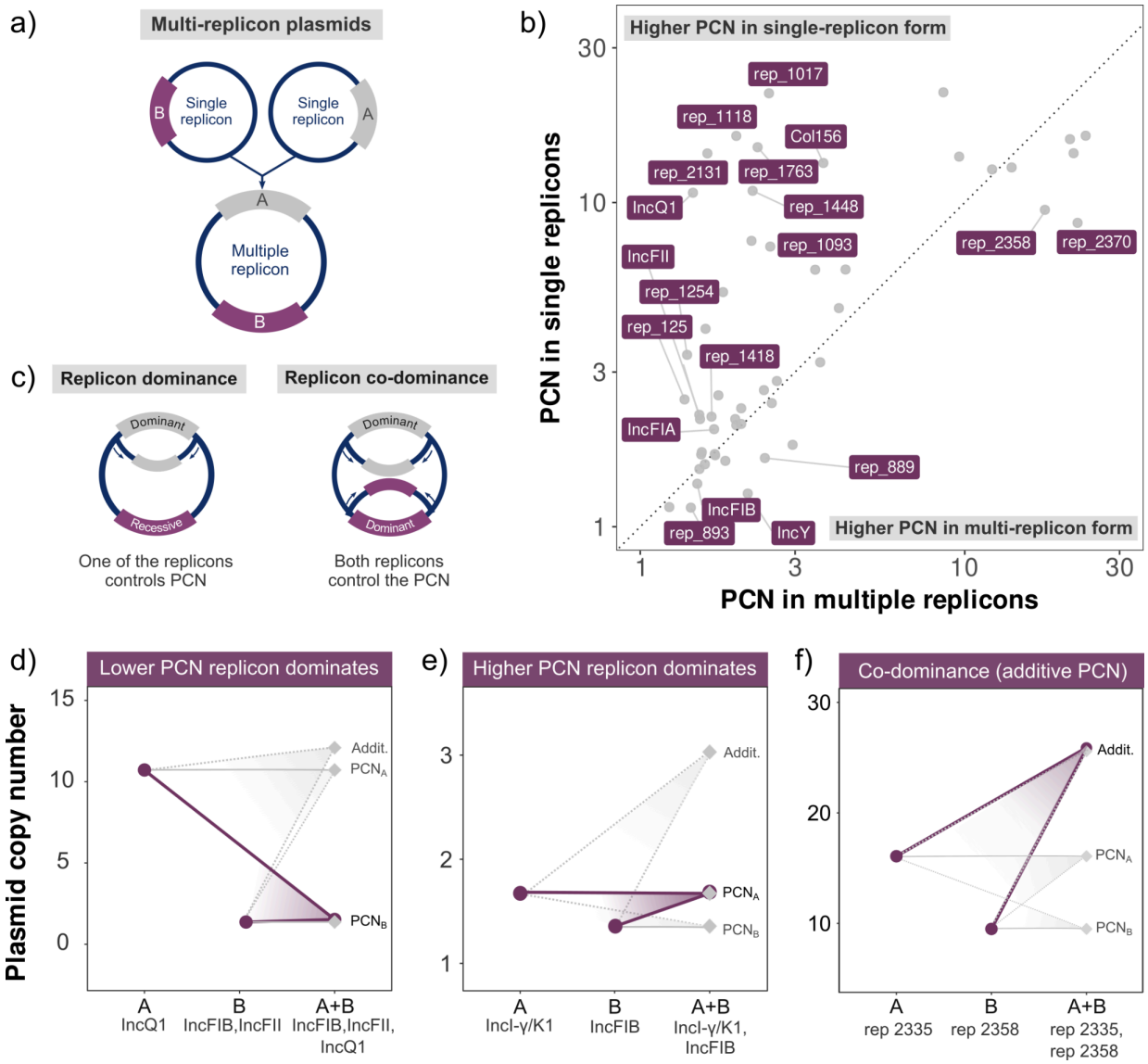

Figure 4. Replicon dominance determines the plasmid copy number of multi-replicon plasmids. a) Scheme depicting the formation of a multi-replicon (co-integrated) plasmid. **b)** Acquisition of additional replicons frequently alters PCN. For each replicon type, the PCN of plasmids as single-replicon (y-axis) is plotted against their PCN when co-existing with other replicons in a multi-replicon plasmid (x-axis). The dotted line indicates no change in PCN between forms. Replicon types with significant PCN differences between single- and multi-replicon forms are labelled ($p < 0.047$; Wilcoxon rank sum test with continuity correction). **c)** Mechanisms controlling PCN in multi-replicon plasmids. The diagram on the left depicts *replicon dominance*, where one replicon ("dominant") exerts full control over the PCN, while the other ("recessive") has no influence. The diagram on the right depicts *co-dominance* between the two replicons, where both contribute to the final PCN. Examples where the replicon with lower or higher PCN is dominant are shown in panels **d)** and **e)**, respectively. **f)** Example of a co-dominance interaction. Grey points depicted predicted dominance outcomes: PCN additivity, or dominance of the higher (A) or lower (B) PCN replicon. Observed data (in purple) depicts the actual PCN scenario for each case. Dots indicate the median PCN. Raw data for each replicon is available in **Extended Data Fig. 12.**

An interesting case of replicon dominance occurs when both replicons are co-dominant, resulting in an additive PCN (**Figure 4c,f, Extended Data Fig. 13**). We found co-dominance exclusively in plasmids carrying Col-like replicons, indicating that it is a specific feature of plasmids of this group. Indeed, a relatively small number of mutations can lead to additive PCN in single-replicon coexisting Col-like plasmids[28,32], suggesting that independence (orthogonality) between plasmid replication systems explains replicon co-dominance (**Extended Data Figs. 12-14**). We also observed other interactions, such as incomplete dominance (resulting in intermediate PCN) or antagonism between replicons. However, due to weak statistical support and the small number of cases, we refrain from discussing them in detail (**Extended Data Fig. 12**).

A pervasive scaling law rules plasmid biology

Next, we sought to identify which factors determine PCN using a random forest regression model. Random forest regressors are supervised machine learning algorithms that leverage ensembles of decision trees to predict continuous variables. To train and refine our model, we used numerical and categorical variables from our dataset (methods). The model could predict PCN using these variables, although with modest performance (**Extended Data Fig. 15**, Mean Absolute Error (MAE): 5.18, R^2: 0.51). Interestingly, plasmid size was the variable that held more predictive power in our dataset (Gini feature importance = 40%), well above other features typically associated with PCN (e.g., PTU or plasmid mobility; Gini feature importance ≤ 10%; **Extended Data Fig. 15**).

Indeed, plasmid size and copy number were strongly and negatively associated (**Extended Data Fig. 16**), and their relationship followed a power law (being linear in a $\log_{10}$-$\log_{10}$ plot; **Figure 5a**). Power laws are typically defined by the formula $y = c \cdot x^k$, which, in this case, takes the following form: $PCN = c \cdot length^k$, where c is the intercept, and k is the scaling factor or slope. The slope was k = -0.65 (95% CI: -0.66, -0.63), indicating that, on average, a 1% increase in size is associated with a 0.65% decrease in PCN (**Supplementary dataset 6**).

This suggests that a scaling law drives the relationship between size and PCN. Scaling laws are prevalent in many natural systems, revealing patterns and relationships across orders of magnitude. In biology, scaling laws typically take k values of ⅔ or ¾ and can be leveraged as powerful tools for modelling and understanding complex systems[33,34]. Some examples of scaling laws include the relationship between metabolic rate and body size in animals and plants[35,36], and the scaling of gene content with regulatory networks in bacterial genomes[37].

To test the universality of the $k \approx -0.65$ (i.e., $k = ⅔$) relationship, we calculated k for each genus in our dataset. Although plasmids from Gram-negative and -positive bacteria are very diverse, copy numbers and plasmid sizes scaled similarly. Indeed, all genera presented slopes not significantly different to k = -0.65 (One-sample t-test, BH adjusted $p > 0.51$ in all cases, **Figure 5a, Extended Data Fig. 17** and **Supplementary dataset 6**). The conservation of k values across bacterial groups further highlights the universality of the PCN-size scaling law and provides a simple formula to roughly estimate the PCN of any plasmid (see methods).

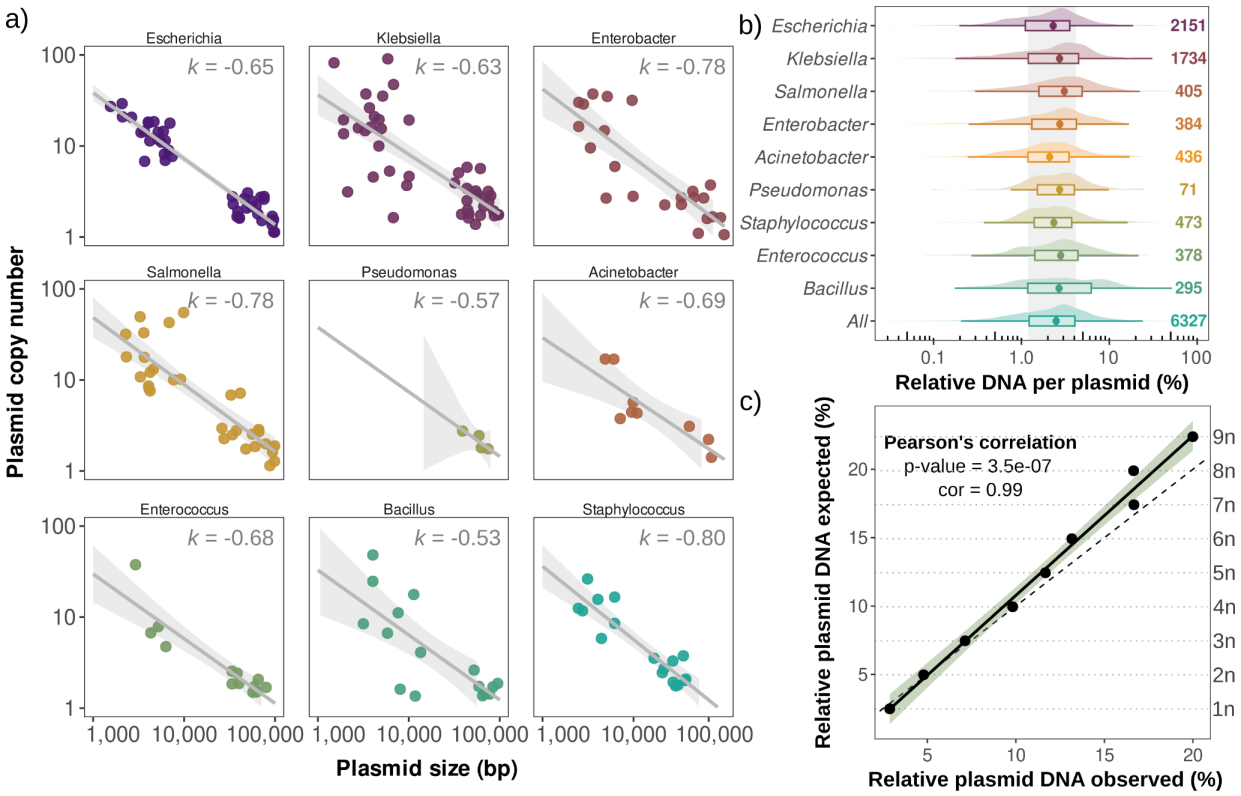

Figure 5. A scaling law links copy number and plasmid size across bacterial phylogeny. a) Scatter plots showing the correlation between plasmid size (x-axis) and PCN (y-axis) for the analyzed genera. Each point represents the median PCN and size for each PTU. Grey lines represent ordinary least squares regression, with the surrounding shaded area indicating 95% confidence intervals. The scaling factor or slope, *k*, is indicated on each panel. **b)** Distribution of total DNA load per plasmid (x-axis) relative to chromosome size per genus (y-axis). The DNA load of each plasmid is calculated by multiplying the plasmid size by the copy number, and then expressed as a proportion relative to the chromosome size. **c)** Correlation of observed (x-axis) and expected (y-axis) plasmid DNA load. Observed data is calculated as the median plasmid DNA load (%) inside a cell when contains 1 plasmid (1n), 2 plasmids (2n), and so on. The expected data has been calculated by generating a sequence from 1 to 9 multiplied by the median of the DNA load per plasmid (2.49%).

Plasmid DNA load is conserved relative to chromosomal size

To shed light on the metabolic constraints imposed by plasmids, we calculated the total DNA content of each plasmid as the product of copy number and size. This reflects the total amount of DNA (in bp) of a given plasmid within a cell or its *DNA load*. Plasmids from *Pseudomonas*, *Bacillus,* and *Salmonella*, and *Klebsiella* accounted for greater DNA loads than average, while the reverse was observed for plasmids from *Acinetobacter*, *Staphylococcus*, and *Enterococcus* (**Extended Data Fig. 18,** Kruskal-Wallis test followed by Dunn's test for pairwise multiple comparisons $p < 10^{-3}$).

We wondered whether variation in chromosome size could explain differences in plasmid DNA load across genera, particularly given that chromosome and plasmid size correlate[2,38]. Our analysis revealed that, regardless of their host genus, size, or copy number, all plasmids accounted for approximately the same percentage of chromosomal DNA (median = 2.49 %, IQR: 1.22-4.06, **Figure 5b,** only *Escherichia* and *Salmonella* being different, albeit negligibly, from “All”; Kruskal-Wallis test followed by Dunn's test for pairwise multiple comparisons p <

10^{-4}). This conserved *relative plasmid DNA load* indicates that common constraints control the interplay between copy number and size in HCPs and LCPs.

Given that PCN is independent of co-resident plasmids (**Supplementary Dataset 6**), we checked whether relative plasmid DNA load scales proportionally to the number of plasmids within the cell. Thus, if any given plasmid accounts for ~2.5% of the genome, the cumulative plasmid DNA load in a cell would be the product of that DNA fraction by the number of plasmids. As such, a cell harbouring two different plasmids would have a relative plasmid DNA content of 2n (~5%), a cell with three plasmids would have 3n (~7.5%), and so on. Remarkably, this expectation correlates almost perfectly with the observed percentage of DNA content allocated to plasmids (Pearson product-moment correlation R^2=0.99, $p < 10^{-6}$; **Figure 5c**). Therefore, the proportion of plasmid DNA within any bacterial cell, indeed, follows a discrete pattern.

Discussion

Copy number is an essential feature of plasmid biology. PCN not only determines a fundamental division between plasmid lifestyles but also drives key differences in gene expression, metabolic burden, and antibiotic resistance[1,11,12,39]. In this work, we leveraged sequencing data to obtain, for the first time, a large-scale dataset of the copy number of 6,327 plasmids (**Figure 1**). We found that PCN varied widely, ranging from ~1 to more than 1,000 copies per cell and that it was generally bimodally distributed. This reflects two well-known plasmid lifestyles, for which a clear distinction was lacking[15,40,41] (**Figure 2**). PCN was generally independent of the content and identity of the plasmid's genetic repertoire (**Extended Data Fig. 5**), the presence of co-resident plasmids (**Supplementary Dataset 5**), and the bacterial host (**Extended Data Fig. 6 and 7**). These results demonstrate that most plasmids encode robust intrinsic replication control mechanisms that determine their characteristic PCN. However, the stringency of PCN control is different between plasmid lifestyles, and naturally occurring HCPs show more variation in PCN than LCPs (**Figure 3**). Moreover, we devised the concept of replicon dominance and used it to explain the interactions defining PCN in widespread multi-replicon plasmids (**Figure 4**).

Arguably, the most intriguing result of our work is that a PCN-size scaling law governs plasmid biology across phylogenetic boundaries (**Figure 5**). This result is further supported by a recent work identifying a consistent scaling law holding across ecological niches[42], indicating that universal constraints orchestrate the PCN-size trade-off. However, the underlying molecular mechanism remains to be uncovered. Plasmid replication might be constrained by a limitation in cellular resources, such as metabolites (e.g., nucleotides), cell machinery (e.g., polymerases and helicases), or even physical intracellular space. Nevertheless, we found that the presence of multiple co-resident plasmids does not affect PCN and that each plasmid independently accounts for a similar DNA load (~2.5% of the chromosome size; **Figure 5**). This suggests that rather than the availability of cellular resources, the efficiency (e.g., replication rates or the turnover of assembled replisomes)[43], regulation (e.g., in response to cellular biomass, cell cycle or culture growth phase)[44] or timing (e.g., synchronicity with the cell-cycle)[45,46] of biophysical processes within the cell might explain the PCN-size scaling law.

Altogether, our comprehensive analysis uncovers the principles that drive PCN. From an applied perspective, leveraging these principles will enhance the design of plasmids as biotechnological tools while also providing a method to predict PCN, which will be useful to, for

instance, improve the assembly of plasmid sequences from metagenomic samples. From a fundamental standpoint, our study provides a detailed catalogue of PCNs across plasmid groups, highlighting the major sources of variability and paving the way for understanding the fundamental constraints that govern plasmid biology.

Materials and Methods

Data processing

Raw reads and assemblies were downloaded from the NCBI database using the sra-toolkit (https://github.com/ncbi/sra-tools) with a custom pipeline (https://github.com/PaulaRamiro/NpAUREO/). Briefly, assemblies were selected based on NCBI's metadata by first selecting specific genera and then filtering according to topology (keeping only circular genomes). We focused on nine different genera from both Gram-negative and -positive bacteria (*Acinetobacter*, *Bacillus*, *Enterobacter*, *Enterococcus*, *Escherichia*, *Klebsiella*, *Pseudomonas*, *Salmonella* and *Staphylococcus*), which include species with biotechnological and clinical interest, such as all members of the ESKAPEE group[17]. SRA information was extracted to download paired-end reads for those assemblies with deposited reads. Assemblies without plasmids were excluded from the analysis. Reads were mapped against their respective assemblies to extract the trimmed-mean coverage using CoverM v0.6.1 (https://github.com/wwood/CoverM) with the following arguments: *coverm contig -m trimmed_mean.* The plasmid copy number was then calculated for each sample as the ratio between the coverage of plasmid contigs and the coverage of the chromosome. Furthermore, we confirmed that the PCN values calculated using CoverM were consistent with those reported in other studies, showing a strong correlation between different methods (**Extended Data Fig. 19**)[16,47,48].

Sequences with an absolute coverage below 30 and plasmids with a PCN below one were discarded from the analysis since this may be due to plasmids being present in only a percentage of the population and may cause an underestimation of the copy number. Finally, we successfully estimated the copy number for the 6,327 plasmids (from 95 bacterial host species) described in **Figure 1**.

Plasmid classification

We classified plasmids using three complementary methods. First, we typed plasmids into different incompatibility groups according to their replication mechanism[5,18] using mob_suite v3.1.8 (https://github.com/phac-nml/mob-suite) using the flag *--multi* to type independent plasmids within samples. This method leverages features in the DNA sequences responsible for plasmid replication (e.g., encoding replication initiation proteins) to establish plasmid groups whose replication is mechanistically similar, termed replicon types.

Second, we used a classification scheme based on similarity across the whole plasmid genetic content with COPLA[19]. Plasmids that share high homology (>70%) in more than 50% of their sequence are assigned to the same plasmid taxonomic unit (PTU)[19,49]. Although PTUs and replicon types were strongly associated (**Extended Data Fig. 20**), we could assign a replicon type to nearly 90% of the plasmids, but only 63% belonged to defined PTUs **(Supplementary**

Dataset 2). Indeed, nearly 4% of the plasmids belonged to new, still unnamed PTUs, while the rest (32%) could not be accurately classified.

To further complement these classifications, we employed a custom clustering approach: Plasmid sequences were extracted from the FASTA files of all samples and annotated with Bakta (https://github.com/oschwengers/bakta)[50]. A distance matrix using gene-by-gene presence-absence was created using the *accnet* function of PATO (https://github.com/irycisBioinfo/PATO)[51] with a Jaccard distance similarity parameter of 70%. Then, we generated a k-nearest neighbours network (K-NNN) to allow reciprocal connections with k =10 neighbours. Plasmids were clustered from the K-NNN using mclust[52].

PCN Analysis

All analyses were performed in R (v4.1.2). Analysis of the modes for PCN distributions was conducted by first checking the number of modes of the distribution with LaplacesDemon[53] v16.1.6 R package and then using the *locmodes* function from the R package multimode[54] v1.5, which estimates the locations of both modes and antimodes, with default parameters.

To measure PCN variation across our dataset, we calculated the relative standard deviation of PCN, also known as the coefficient of variation (CV), for each plasmid group. The CV allows for comparing the degree of variation from one plasmid group to another, even if the PCNs are drastically different and was calculated by dividing the standard deviation by the mean PCN for each plasmid group.

Plasmid DNA load (bp) was calculated as the product of plasmid size (bp) by PCN. The relative percentage of plasmid DNA load was calculated as (plasmid size (bp) / chromosome length (bp)) x 100.

Replicon dominance analysis

To visualize the statistical significance of differences in PCN between groups, we employed a letter-based classification using the *cldList* function from the rcompanion R package[55]. *cldList* was used to assign letters to each group based on the p-values for the Dunn test performed after the Kruskal-Wallis test (see Statistical analysis and regression). Groups without statistically significant differences were excluded from the analysis. In cases where the multi-replicon form was not different from only one of the simple replicons (e.g. 'a', 'a', 'b'), it was identified as a case of *dominance*. Other occurrences, such as ('a', 'ab', and 'b'), or ('a', 'b', and 'c'), were classified as “other interactions”.

We then checked cases where the multi-replicon form had a higher median PCN than each single form, to find cases of *co-dominance*. In those cases, to obtain statistical support and test for an additive effect, we generated a bootstrap distribution representing the sum of the single replicons and compared it to the observed values. We excluded *co-dominance* cases when the PCN of the multi-replicon and that of the bootstrap were significantly different.

Model training

To train the prospective model, manual curation of the dataset was performed first to remove redundant or non-informative variables for PCN (e.g., Species). Also, categorical variables

with too many classes were eliminated if other variables contained the same information with fewer classes. The final list of variables used to train the model was as follows: genus, predicted mobility, the presence of single or multiple replicons, length of the chromosome of the host, GC content of the plasmid, number of plasmids present in the host, predicted PTU, and size of the plasmid (with a $\log_{10}$ transformation). The output variable was PCN. Observations with PCNs > 100 were considered outliers and eliminated. Observations with unknown or not assigned PTUs were also eliminated to suppress noise in the dataset.

Several models, including simple linear regression[56], generalised linear models[56], XGboost[57], elastic net regressor[56], multi-layer perceptron regressor[56] and random forest regressor[56] were pre-tested with light tuning. In all trials, sklearn-RandomForestRegressor outperformed all other models. After selecting RandomForestRegressor, further tuning was performed: first, a random search cross-validation with a wide parameter range (initial parameters available in the code repository), and then, a deeper grid search cross-validation with values around the parameters selected in the random search. Finally, recursive feature elimination was used to improve the final model using mean absolute error as the performance metric. Gini Feature importance was directly extracted from the model using the built-in function. The complete code and dataset used for the final model are available at https://github.com/PaulaRamiro/NpAUREO/tree/main/Model.

Statistical analyses

The significance level was set at 0.05 for all statistical tests. All statistical tests performed were two-tailed. In all boxplots, the box size extends to the interquartile range (IQR), and the line represents the median. Whiskers extend from the edges of the box to the smallest and largest values within 1.5 times the IQR. Outliers are plotted as individual points beyond the whiskers.
The Chi-squared test was used to compare the counts of HCPs and LCPs of each genera against the total population to reveal significant over or underrepresentation of either.
When data did not meet the assumptions for a one-way ANOVA (normal distribution and homoscedasticity), the Kruskal-Wallis test was used to compare multiple groups. Dunn's test was further performed to determine which groups presented statistically significant differences.
To compare two single independent groups, we employed the Wilcoxon rank-sum test with continuity correction. In cases of multiple testing, we used the Benjamini-Hochberg (BH) correction to control for the false discovery rate.
Spearman correlation analysis was used in all cases where the assumptions of Pearson correlation (continuity, linearity, heteroscedasticity, and normality) were not met. Otherwise, Pearson's correlation was used.
For regressions regarding the scaling law, given the assumption that the source of error is predominantly the dependent variable (PCN) rather than the independent variable (plasmid size), we employed ordinary least squares (OLS) regression for all fits of log-transformed data. This approach is consistent with other published analyses for this type of data[58,59]. The median PCN per each PTU was used to calculate the slopes for each genus. To assess the statistical significance between the slopes of different genera, we fitted OLS with an interaction term for Genus and performed pairwise comparisons among all genera.

Author contributions

PR-M and IdQ analyzed the data and created the figures. JAG and JR-B gave technical support and conceptual advice. PR-M and JR-B conceived the project. JR-B supervised the project. All authors discussed and provided critical feedback during the analysis of results. All authors wrote, edited, and reviewed the manuscript.

Acknowledgements

We thank Teresa M. Coque and Val F. Lanza for their suggestions. Work in the evodynamics lab (https://evodynamicslab.com/) is supported by project no. PI21/01363, funded by the Carlos III Health Institute (ISCIII) and co-funded by the European Union; CIBER —Consorcio Centro de Investigación Biomédica en Red— (CIBERINFEC) CB21/13/00084; Convocatoria SEIMC-FUNDACIÓN SORIA MELGUIZO de Investigación 2021; and funded by the European Union (ERC, HorizonGT, 101077809). Views and opinions expressed are, however, those of the author(s) only and do not necessarily reflect those of the European Union or the European Research Council Executive Agency. Neither the European Union nor the granting authority can be held responsible for them. PRM is a recipient of a predoctoral PFIS grant (grant no. FI22/00265) from the Carlos III Health Institute (ISCIII), through the Recovery, Transformation and Resilience Plan and Next Generation EU from the European Union. JR-B acknowledges support by a Miguel Servet contract from the Carlos III Health Institute (ISCIII) (grant no. CP20/00154), co-founded by the European Social Fund, 'Investing in your future'.

Competing interests

The authors declare no competing interests.

References

1. Rodríguez-Beltrán, J., DelaFuente, J., León-Sampedro, R., MacLean, R. C. & San Millán, Á. Beyond horizontal gene transfer: the role of plasmids in bacterial evolution. *Nat. Rev. Microbiol.* **19**, 347–359 (2021).
2. Smillie, C., Garcillán-Barcia, M. P., Francia, M. V., Rocha, E. P. C. & de la Cruz, F. Mobility of plasmids. *Microbiol. Mol. Biol. Rev. MMBR* **74**, 434–52 (2010).
3. Coluzzi, C., Garcillán-Barcia, M. P., De La Cruz, F. & Rocha, E. P. C. Evolution of Plasmid Mobility: Origin and Fate of Conjugative and Nonconjugative Plasmids. *Mol. Biol. Evol.* **39**, msac115 (2022).
4. Del Solar, G., Giraldo, R., Ruiz-Echevarría, M. J., Espinosa, M. & Díaz-Orejas, R. Replication and Control of Circular Bacterial Plasmids. *Microbiol. Mol. Biol. Rev.* **62**, 434–464 (1998).
5. Shintani, M., Sanchez, Z. K. & Kimbara, K. Genomics of microbial plasmids: classification and identification based on replication and transfer systems and host taxonomy. *Front. Microbiol.* **6**, (2015).
6. Almpanis, A., Swain, M., Gatherer, D. & McEwan, N. Correlation between bacterial G+C content, genome size and the G+C content of associated plasmids and bacteriophages. *Microb. Genomics* **4**, (2018).
7. Novick, R. P. Plasmid incompatibility. *Microbiol. Rev.* **51**, 381–395 (1987).
8. Sengupta, M. & Austin, S. Prevalence and Significance of Plasmid Maintenance Functions in the Virulence Plasmids of Pathogenic Bacteria. *Infect. Immun.* **79**, 2502–2509 (2011).
9. San Millan, A. Evolution of Plasmid-Mediated Antibiotic Resistance in the Clinical Context. *Trends Microbiol.* **26**, 978–985 (2018).
10. Nicoloff, H., Hjort, K., Andersson, D. I. & Wang, H. Three concurrent mechanisms generate gene copy number variation and transient antibiotic heteroresistance. *Nat. Commun.* **15**, 3981 (2024).
11. Nicoloff, H., Hjort, K., Levin, B. R. & Andersson, D. I. The high prevalence of antibiotic heteroresistance in pathogenic bacteria is mainly caused by gene amplification. *Nat.*

Microbiol. **4**, 504–514 (2019).

12. Hernandez-Beltran, J. C. R. *et al.* Plasmid-mediated phenotypic noise leads to transient antibiotic resistance in bacteria. *Nat. Commun.* **15**, 2610 (2024).
13. San Millan, A., Escudero, J. A., Gifford, D. R., Mazel, Di. & MacLean, R. C. Multicopy plasmids potentiate the evolution of antibiotic resistance in bacteria. *Nat. Ecol. Evol.* **1**, 1–8 (2016).
14. Ilhan, J. *et al.* Segregational Drift and the Interplay between Plasmid Copy Number and Evolvability. *Mol. Biol. Evol.* **36**, 472–486 (2019).
15. Friehs, K. Plasmid Copy Number and Plasmid Stability. in *New Trends and Developments in Biochemical Engineering* (ed. Scheper, T.) vol. 86 47–82 (Springer Berlin Heidelberg, Berlin, Heidelberg, 2004).
16. Shaw, L. P. *et al.* Niche and local geography shape the pangenome of wastewater- and livestock-associated Enterobacteriaceae. *Sci. Adv.* **7**, eabe3868 (2021).
17. Yu, Z., Tang, J., Khare, T. & Kumar, V. The alarming antimicrobial resistance in ESKAPEE pathogens: Can essential oils come to the rescue? *Fitoterapia* **140**, 104433 (2020).
18. Robertson, J. & Nash, J. H. E. MOB-suite: software tools for clustering, reconstruction and typing of plasmids from draft assemblies. *Microb. Genomics* **4**, (2018).
19. Redondo-Salvo, S. *et al.* COPLA, a taxonomic classifier of plasmids. *BMC Bioinformatics* **22**, 390 (2021).
20. Ares-Arroyo, M., Rocha, E. P. C. & Gonzalez-Zorn, B. Evolution of ColE1-like plasmids across γ-Proteobacteria: From bacteriocin production to antimicrobial resistance. *PLOS Genet.* **17**, e1009919 (2021).
21. Garcia-Migura, L., Hasman, H. & Jensen, L. B. Presence of pRI1: A Small Cryptic Mobilizable Plasmid Isolated from Enterococcus faecium of Human and Animal Origin. *Curr. Microbiol.* **58**, 95–100 (2009).
22. Fernández-López, C. *et al.* Mobilizable Rolling-Circle Replicating Plasmids from Gram-Positive Bacteria: A Low-Cost Conjugative Transfer. *Microbiol. Spectr.* **2**, 2.5.15 (2014).

23. Tinsley, E., Naqvi, A., Bourgogne, A., Koehler, T. M. & Khan, S. A. Isolation of a Minireplicon of the Virulence Plasmid pXO2 of *Bacillus anthracis* and Characterization of the Plasmid-Encoded RepS Replication Protein. *J. Bacteriol.* **186**, 2717–2723 (2004).
24. Weaver, K. E., Kwong, S. M., Firth, N. & Francia, M. V. The replicons of Gram-positive bacteria: A family of broadly distributed but narrow host range plasmids. *Plasmid* **61**, 94–109 (2009).
25. Clewell, D. B. *et al.* Extrachromosomal and Mobile Elements in Enterococci: Transmission, Maintenance, and Epidemiology. in *Enterococci: From Commensals to Leading Causes of Drug Resistant Infection* (eds. Gilmore, M. S., Clewell, D. B., Ike, Y. & Shankar, N.) (Massachusetts Eye and Ear Infirmary, Boston, 2014).
26. Firth, N., Jensen, S. O., Kwong, S. M., Skurray, R. A. & Ramsay, J. P. Staphylococcal Plasmids, Transposable and Integrative Elements. *Microbiol. Spectr.* **6**, 6.6.06 (2018).
27. San Millan, A., Heilbron, K. & MacLean, R. C. Positive epistasis between co-infecting plasmids promotes plasmid survival in bacterial populations. *ISME J.* **8**, 601–612 (2014).
28. Santos-Lopez, A. *et al.* Compensatory evolution facilitates the acquisition of multiple plasmids in bacteria. Preprint at https://doi.org/10.1101/187070 (2017).
29. Jahn, M., Günther, S. & Müller, S. Non-random distribution of macromolecules as driving forces for phenotypic variation. *Curr. Opin. Microbiol.* **25**, 49–55 (2015).
30. Jahn, M., Vorpahl, C., Hübschmann, T., Harms, H. & Müller, S. Copy number variability of expression plasmids determined by cell sorting and Droplet Digital PCR. *Microb. Cell Factories* **15**, 211 (2016).
31. Douarre, P.-E., Mallet, L., Radomski, N., Felten, A. & Mistou, M.-Y. Analysis of COMPASS, a New Comprehensive Plasmid Database Revealed Prevalence of Multireplicon and Extensive Diversity of IncF Plasmids. *Front. Microbiol.* **11**, 483 (2020).
32. Santos-Lopez, A. *et al.* A Naturally Occurring Single Nucleotide Polymorphism in a Multicopy Plasmid Produces a Reversible Increase in Antibiotic Resistance. *Antimicrob. Agents Chemother.* **61**, e01735-16 (2017).
33. Savage, V. M. *et al.* The predominance of quarter‐power scaling in biology. *Funct. Ecol.*

18, 257–282 (2004).

34. West, G. B. The Origin of Universal Scaling Laws in Biology.
35. Kleiber, M. Body size and metabolism. *Hilgardia* **6**, 315–353 (1932).
36. Enquist, B. J., Brown, J. H. & West, G. B. Allometric scaling of plant energetics and population density. *Nature* **395**, 163–165 (1998).
37. Beslon, G., Parsons, D. P., Sanchez-Dehesa, Y., Peña, J.-M. & Knibbe, C. Scaling laws in bacterial genomes: A side-effect of selection of mutational robustness? *Biosystems* **102**, 32–40 (2010).
38. Slater, F. R., Bailey, M. J., Tett, A. J. & Turner, S. L. Progress towards understanding the fate of plasmids in bacterial communities: Fate of plasmids in bacterial communities. *FEMS Microbiol. Ecol.* **66**, 3–13 (2008).
39. Maddamsetti, R. *et al.* Duplicated antibiotic resistance genes reveal ongoing selection and horizontal gene transfer in bacteria. *Nat. Commun.* **15**, 1449 (2024).
40. Mayer, M. P. A new set of useful cloning and expression vectors derived from pBlueScript. *Gene* **163**, 41–46 (1995).
41. Agaphonov, M. O. *et al.* Vectors for rapid selection of integrants with different plasmid copy numbers in the yeastHansenula polymorpha DL1. *Yeast* **15**, 541–551 (1999).
42. Maddamsetti, R. *et al.* Scaling laws of plasmids across the microbial tree of life. Preprint at https://doi.org/10.1101/2024.10.04.616653 (2024).
43. Wegrzyn, K. E., Gross, M., Uciechowska, U. & Konieczny, I. Replisome Assembly at Bacterial Chromosomes and Iteron Plasmids. *Front. Mol. Biosci.* **3**, (2016).
44. Turgeon, N., Laflamme, C., Ho, J. & Duchaine, C. Evaluation of the plasmid copy number in B. cereus spores, during germination, bacterial growth and sporulation using real-time PCR. *Plasmid* **60**, 118–124 (2008).
45. Keasling, J. D., Palsson, B. O. & Cooper, S. Cell-cycle-specific F plasmid replication: regulation by cell size control of initiation. *J. Bacteriol.* **173**, 2673–2680 (1991).
46. Fournes, F., Val, M.-E., Skovgaard, O. & Mazel, D. Replicate Once Per Cell Cycle: Replication Control of Secondary Chromosomes. *Front. Microbiol.* **9**, 1833 (2018).

47. Roosaare, M., Puustusmaa, M., Möls, M., Vaher, M. & Remm, M. PlasmidSeeker: identification of known plasmids from bacterial whole genome sequencing reads. *PeerJ* **6**, e4588 (2018).
48. Jangir, P. K. *et al.* Pre-existing chromosomal polymorphisms in pathogenic E. coli potentiate the evolution of resistance to a last-resort antibiotic. *eLife* **11**, e78834 (2022).
49. Redondo-Salvo, S. *et al.* Pathways for horizontal gene transfer in bacteria revealed by a global map of their plasmids. *Nat. Commun.* **11**, 3602 (2020).
50. Schwengers, O. *et al.* Bakta: rapid and standardized annotation of bacterial genomes via alignment-free sequence identification: Find out more about Bakta, the motivation, challenges and applications, here. *Microb. Genomics* **7**, (2021).
51. Fernández-de-Bobadilla, M. D. *et al.* PATO: Pangenome Analysis Toolkit. *Bioinformatics* **37**, 4564–4566 (2021).
52. Fraley, C. & Raftery, A. Model-based Methods of Classification: Using the **mclust** Software in Chemometrics. *J. Stat. Softw.* **18**, (2007).
53. Statisticat, LLC. LaplacesDemon: Complete Environment for Bayesian Inference. (2021).
54. Ameijeiras-Alonso, J., Crujeiras, R. M. & Rodriguez-Casal, A. **multimode** : An *R* Package for Mode Assessment. *J. Stat. Softw.* **97**, (2021).
55. Mangiafico, S. rcompanion: Functions to support extension education program evaluation. *R Package Version* **2**, (2020).
56. Pedregosa, F. *et al.* Scikit-learn: Machine Learning in Python. Preprint at http://arxiv.org/abs/1201.0490 (2018).
57. Chen, T. & Guestrin, C. XGBoost: A Scalable Tree Boosting System. in *Proceedings of the 22nd ACM SIGKDD International Conference on Knowledge Discovery and Data Mining* 785–794 (ACM, San Francisco California USA, 2016). doi:10.1145/2939672.2939785.
58. White, E. P., Xiao, X., Isaac, N. J. B. & Sibly, R. M. Methodological Tools. in *Metabolic Ecology* (eds. Sibly, R. M., Brown, J. H. & Kodric‐Brown, A.) 7–20 (Wiley, 2012). doi:10.1002/9781119968535.ch1.
59. Hatton, I. A. *et al.* The predator-prey power law: Biomass scaling across terrestrial and

aquatic biomes. *Science* **349**, aac6284 (2015).

Extended data for

Universal rules govern plasmid copy number

Paula Ramiro-Martínez[1], Ignacio de Quinto[1], João Alves Gama[1], and Jerónimo Rodríguez-Beltrán*[,1,2]

1. Microbiology Department. Hospital Universitario Ramón y Cajal-IRYCIS, Madrid, Spain.
2. Centro de Investigación Biomédica en Red de Enfermedades Infecciosas (CIBERINFEC), Instituto de Salud Carlos III, Madrid, Spain.

* Address correspondence to JR-B: jeronimo.rodriguez.beltran@gmail.com

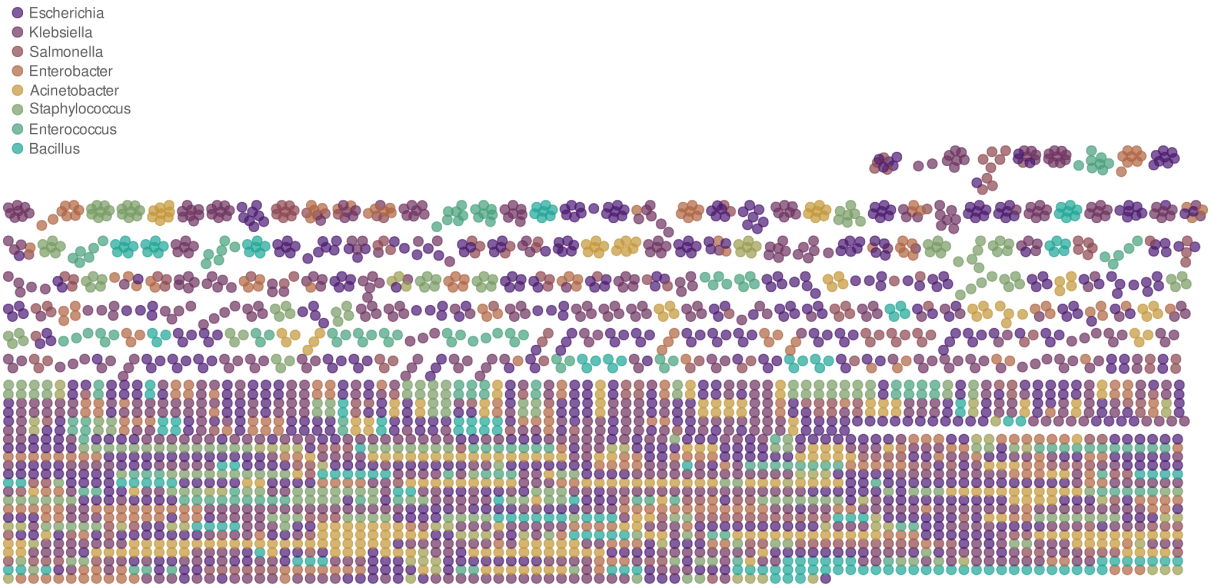

Extended Data Figure 1. Plasmid clusters containing less than ten members.

Plasmid cluster network built with the k-nearest neighbours' algorithm (K-NNN). Each node represents a plasmid, coloured according to the genus of the bacterial host. Only clusters with less than ten plasmids are shown.

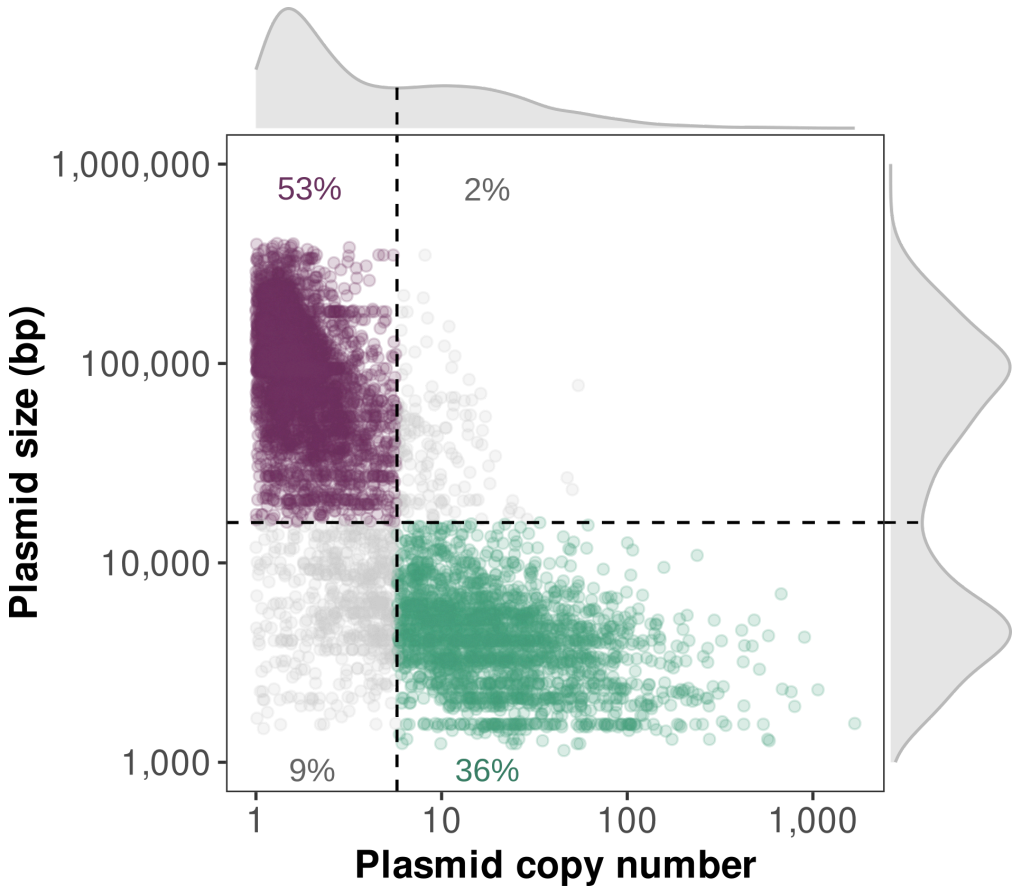

Extended Data Figure 2. Distribution of plasmids according to size and copy number.

Plasmid size (y-axis) and plasmid copy number (x-axis) distributions are shown outside the box. The anti-modes of the distributions for the logarithm of plasmid size (15,939 bp) and plasmid copy number (5.75 copies) are depicted with dashed lines. These limits classify each plasmid in the dataset (individual points) according to its size and copy number. Large LCPs (purple) are represented in the upper-left quadrant, while small HCPs (green) are in the bottom-right quadrant. Large HCPs and small LCPs are depicted in gray in the upper-right and bottom-left quadrants, respectively.

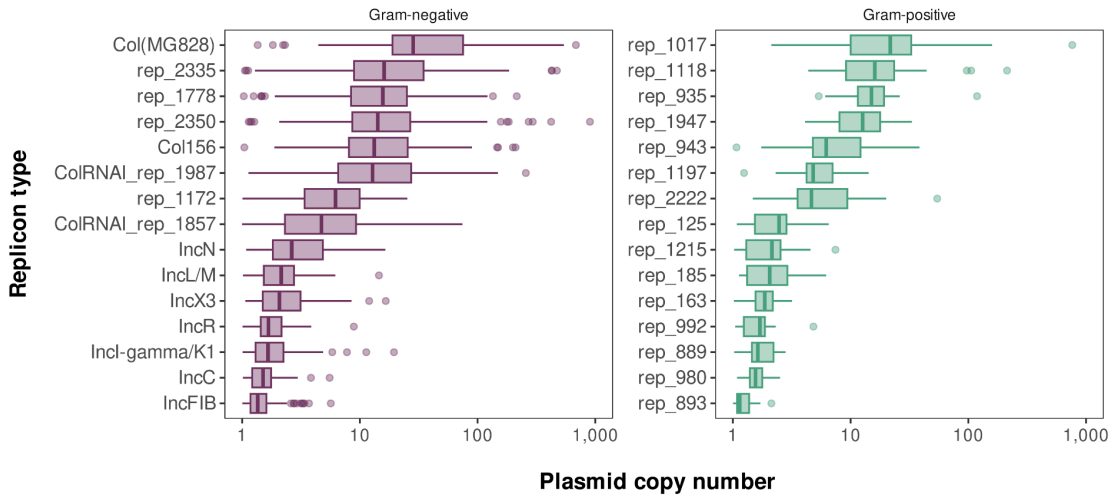

Extended Data Figure 3. Plasmid copy number variability within replicon types.

The boxplots represent plasmid copy number (x-axis) per replicon type (y-axis) in Gram-negative (left panel) and Gram-positive (right panel) bacteria.

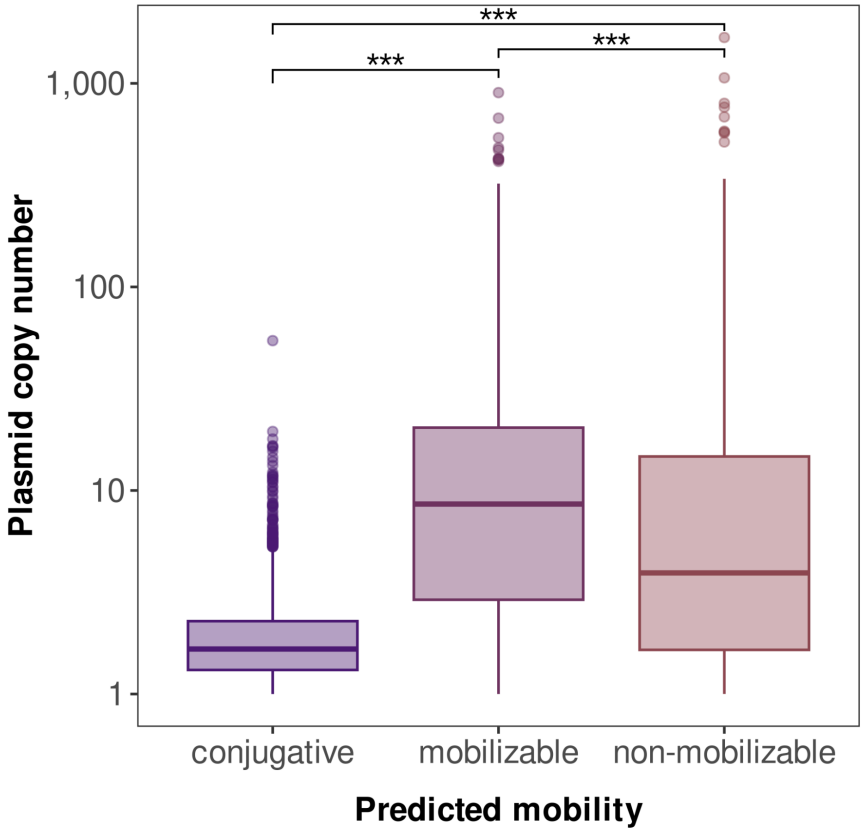

Extended Data Figure 4. Copy number according to plasmid's predicted mobility.

The y-axis represents the plasmid copy number, while the x-axis represents plasmid categories based on predicted mobility: conjugative, mobilizable, and non-mobilizable. Each box plot shows plasmid copy numbers within each category. Statistical significance between groups is indicated by asterisks (Kruskal-Wallis test followed by Dunn's test for pairwise multiple comparisons, $p < 0.00001$).

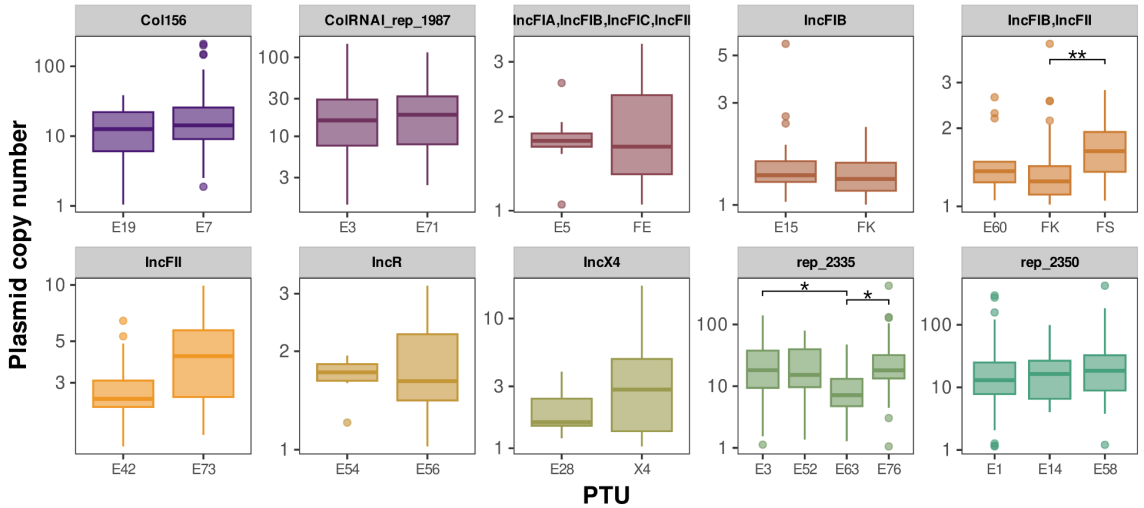

Extended Data Figure 5. Plasmid copy number by PTUs within replicon types.

Boxplots show the plasmid copy number (y-axis) across different PTUs (x-axis) for the most representative plasmid types. Each panel represents a different plasmid type (labeled at the top), with comparisons among its PTUs (labeled on the x-axis). Asterisks denote statistical significance according to Kruskal-Wallis test followed by Dunn's test for pairwise multiple comparisons (* for $p < 0.05$, ** for $p < 0.01$).

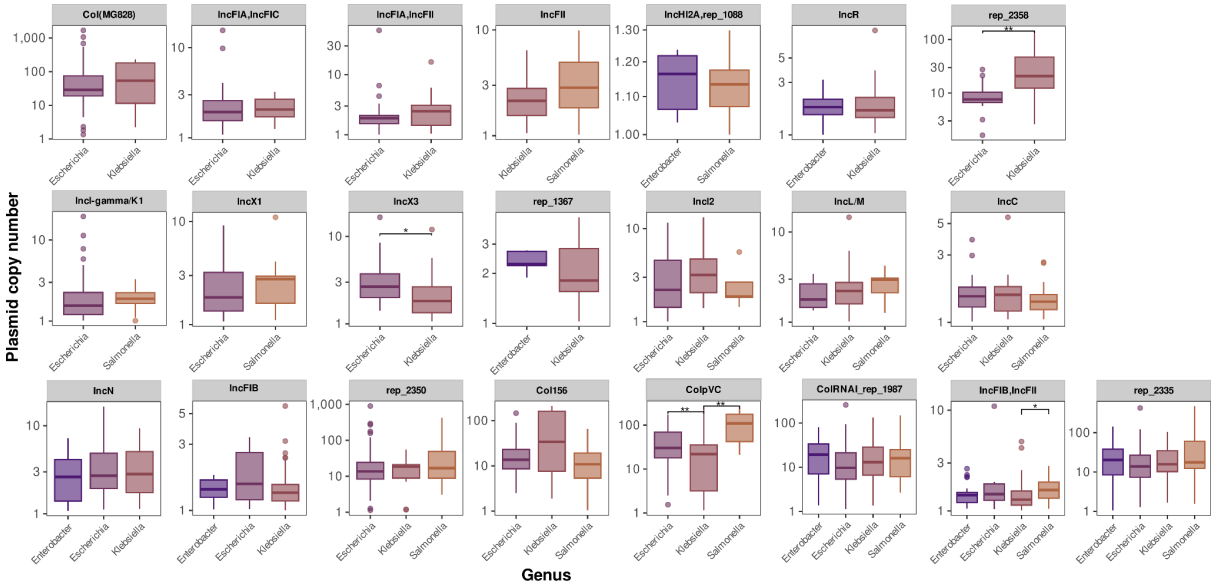

Extended Data Figure 6. Plasmid copy number of replicon types across different hosts.

Boxplots show the plasmid copy number (y-axis) across different hosts (x-axis) for the most representative replicon types in multiple genera. Each panel represents a replicon type (labelled at the top), with comparisons among host genera (labelled on the x-axis). Asterisks denote statistical significance according to the Kruskal-Wallis test, followed by Dunn's test for pairwise multiple comparisons (* for $p < 0.05$, ** for $p < 0.01$).

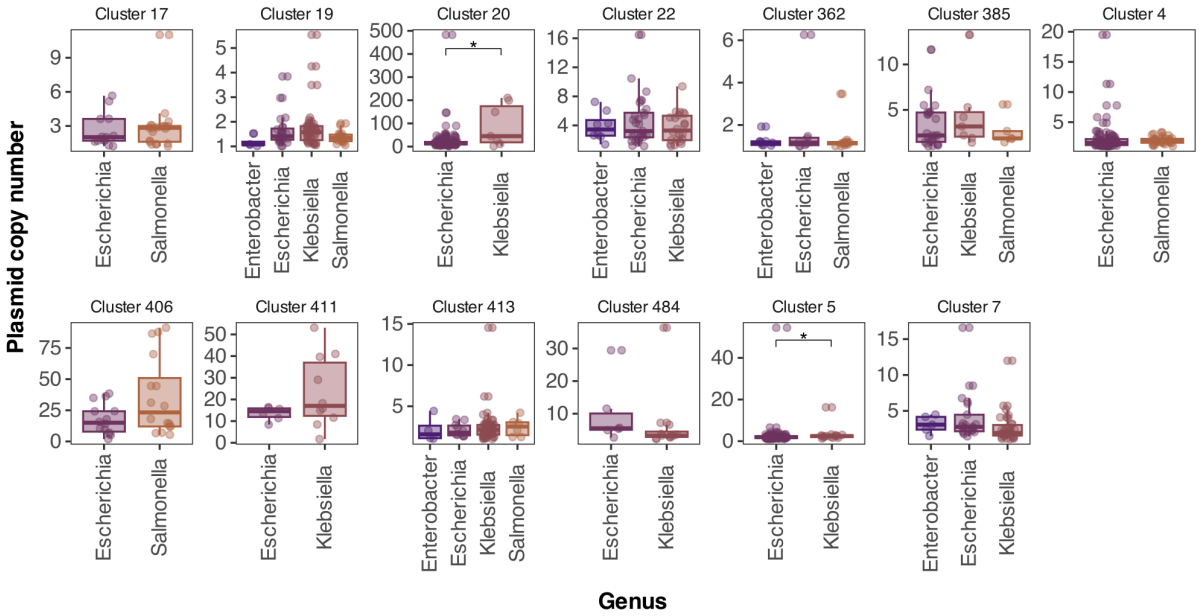

Extended Data Figure 7. Plasmid copy number of plasmid clusters across different hosts.

Boxplots show plasmid copy number (y-axis) distributions per host genus (x-axes) for the most representative clusters present in multiple genera (n >3). Each panel represents a different plasmid cluster (labelled at the top), and each point represents a different plasmid. Asterisks denote statistical significance according to the Wilcoxon rank sum exact test, $p < 0.047$.

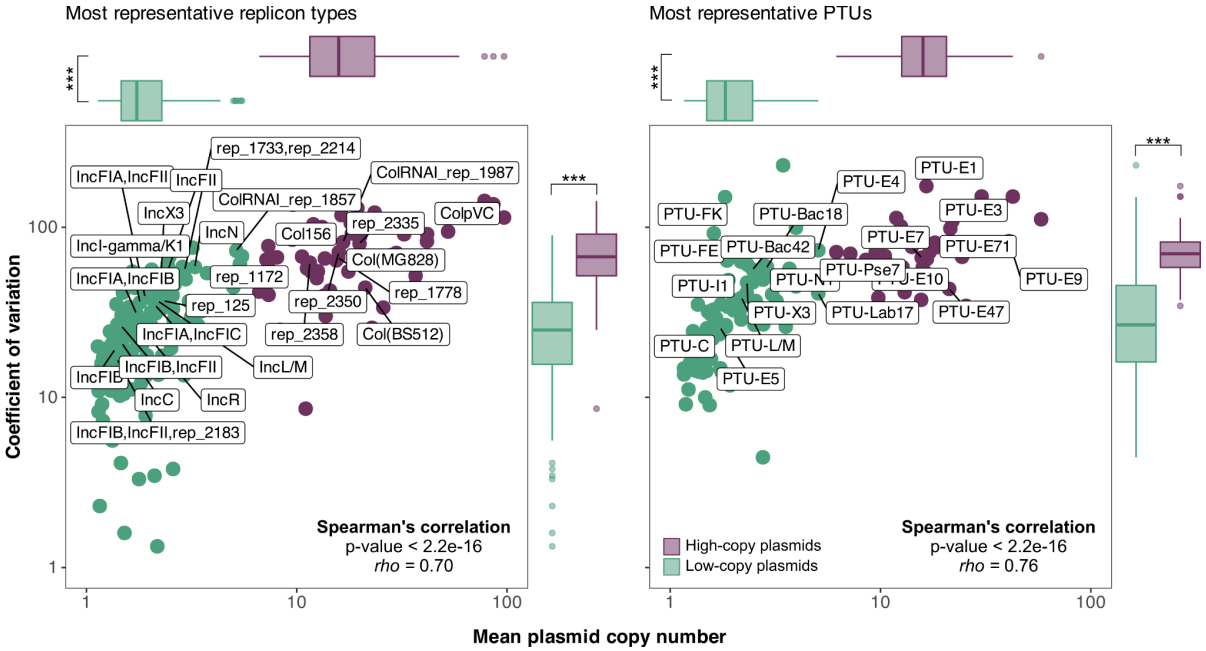

Extended Data Figure 8. Intrinsic PCN variability, estimated without outliers.

The mean PCN (x-axis) is plotted against the coefficient of variation (CV, y-axis), according to replicon type (left) or PTU (right), as in **Figure 3**. Each dot represents the mean PCN and CV of a plasmid group, now estimated without outliers. The Spearman's rho and p-value for each correlation are shown at the bottom right of each plot. Labels indicate the most representative plasmid groups. Colours distinguish HCP (purple) from LCP (green). Boxplots represent aggregated PCN (top) and CV (right) data for all plasmid groups, according to the classification as HCPs and LCPs. Asterisks indicate significant differences between HCP and LCP (*** for $p < 10^{-6}$, Wilcoxon rank sum exact test).

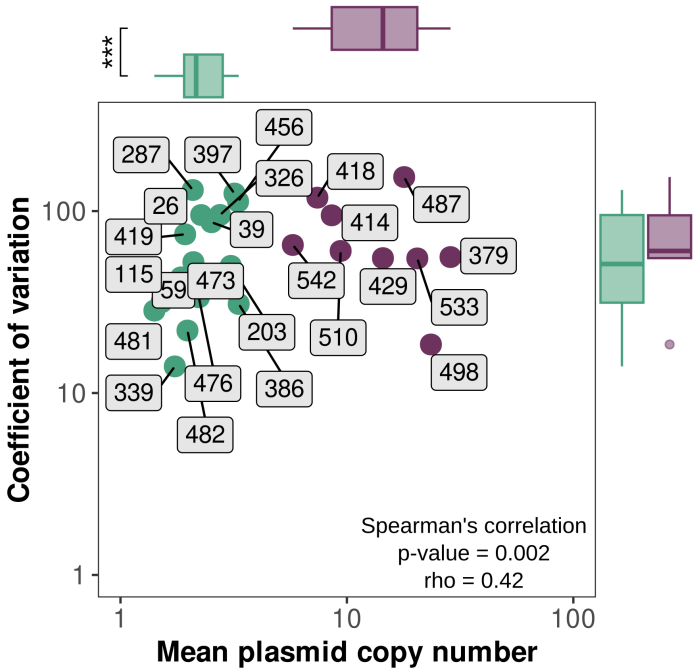

Extended Data Figure 9. Intrinsic PCN variability per plasmid clusters.

Each dot represents the mean PCN (x-axis) and CV (y-axis) for the most representative plasmid clusters. Each cluster is labeled next to the respective point. The Spearman's rho and p-value for the correlation are shown at the bottom right corner. Colours distinguish HCPs (purple) from LCPs (green). Boxplots represent aggregated PCN (top) and CV (right) data for all plasmid groups, according to the classification as HCPs and LCPs. Asterisks indicate significant differences between HCP and LCP (*** for $p < 0.001$, Wilcoxon rank sum exact test).

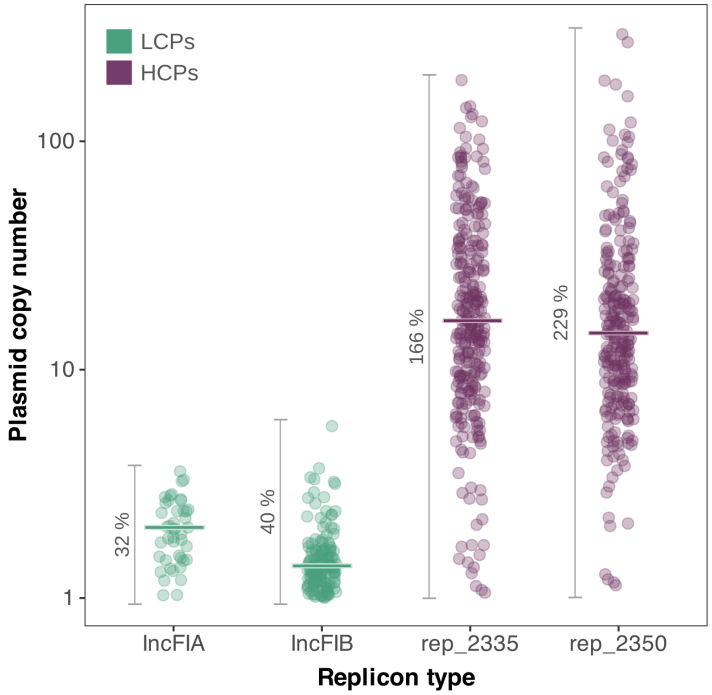

Extended Data Figure 10. Intrinsic PCN variability of replicon types IncFIA, IncFIB, rep_2335, and rep_2350.

The y-axis represents the plasmid copy number, and the x-axis represents replicon types. Colors represent low-copy plasmids (LCPs, green) and high-copy plasmids (HCPs, purple). Horizontal bars indicate the median plasmid copy number for each group. Vertical bars indicate the percentage of variability in plasmid copy number for each replicon type.

Extended Data Figure 11. Variation in PCN between single and multi-replicon forms.

The y-axis represents the plasmid copy number, and the x-axis represents the different plasmid forms: single replicons (orange) and multiple replicons (purple). Asterisks indicate statistically significant differences in PCN between single and multiple replicons (Wilcoxon rank sum exact test, * for $p < 0.05$, ** for $p < 0.01$, *** for $p < 0.001$).

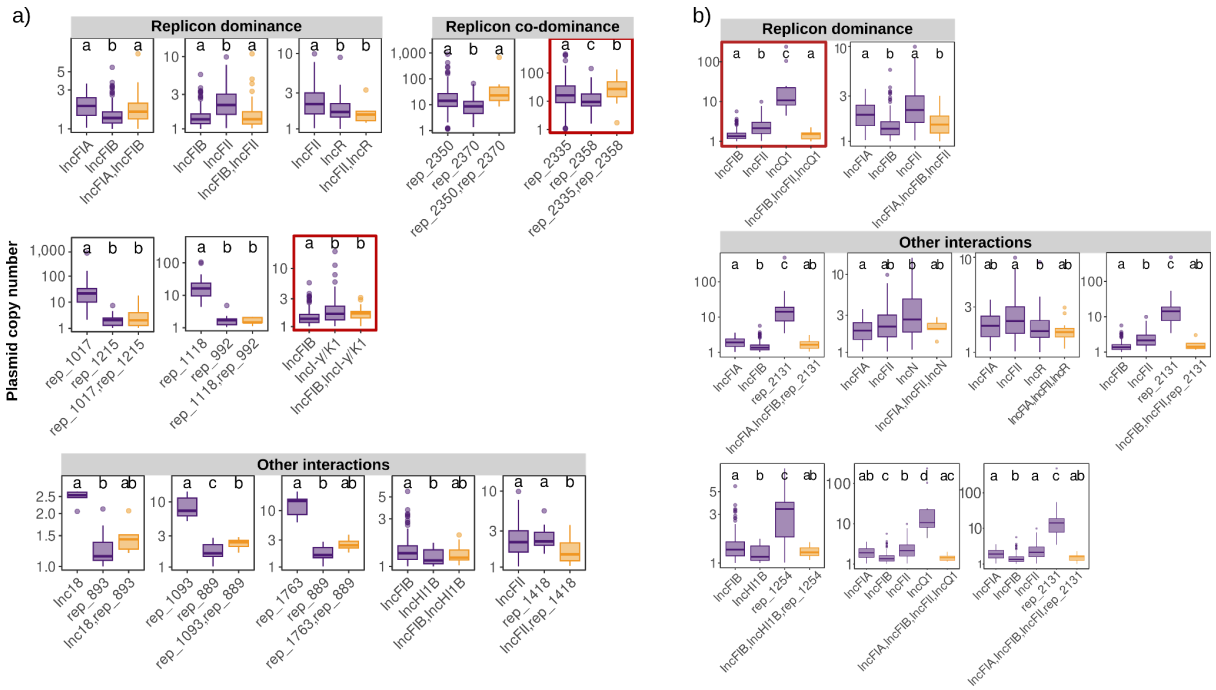

Extended Data Figure 12. Replicon dominance interactions.

Boxplots represent plasmid copy number (y-axes) among different replicons (x-axes) in multi-replicon plasmids: a) composed of only two replicons, b) composed of three-four replicons. Interactions are classified into two groups: “replicon dominance” and “other interactions”. Letters assign groups based on statistical differences from the Dunn test. In cases where the multi-replicon form is not different from only one of the simple replicons, it is identified as a case of dominance. Other occurrences were classified as “other interactions”. Boxes highlighted in red correspond to the examples shown in **Figure 4 d-f**.

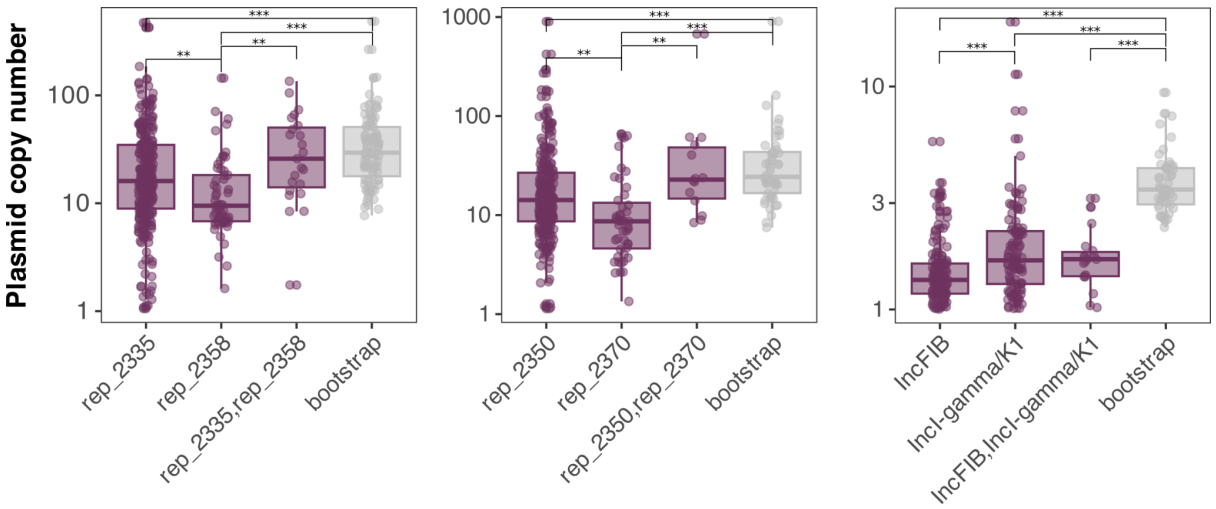

Extended Data Figure 13. Candidate cases of additive effect in PCN due to replicon *co-dominance*.

In each panel, boxplots represent the distribution of PCN (y-axis) for the different replicon states (x-axis): each individual plasmid replicon, the observed PCN for multi-replicon form (rep_2335,rep_2358), and the expected (additive) PCN estimated through bootstrapping (see methods). Asterisks indicate statistically significant differences (Kruskal-Wallis test followed by Dunn's test, ** $p < 10^{-2}$, *** $p < 10^{-3}$).

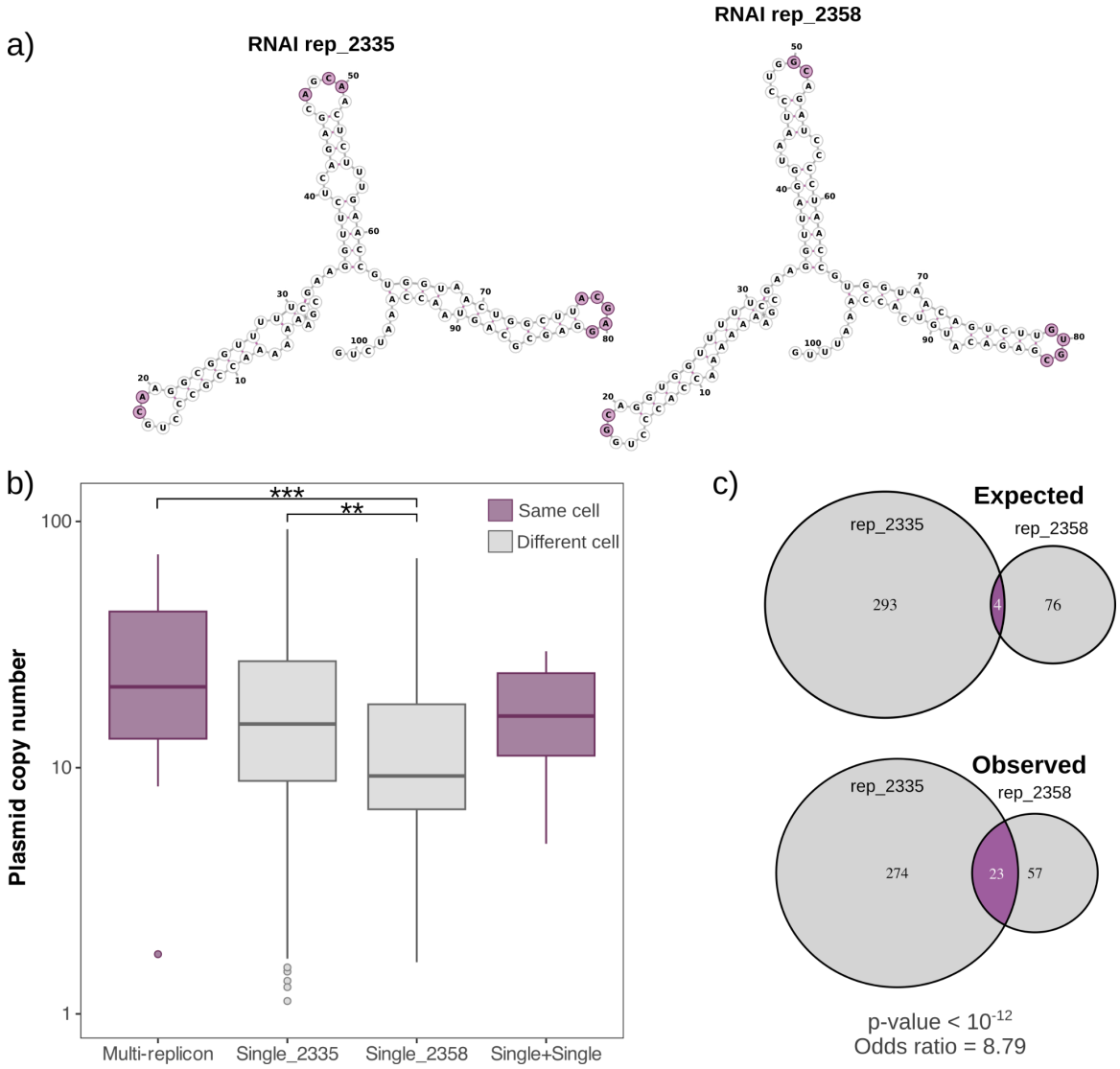

Extended Data Figure 14. Structural analysis and PCN comparison of Col-like plasmids in different forms.

a) Predicted RNAI structures from replicons rep_2335 and rep_2358 of the co-integrate example plasmid. RNAI negatively controls replication initiation in Col-like plasmids through three conserved stem-loops in its secondary structure. Therefore, mutations that affect these loops alter PCN and determine plasmid incompatibility. RNAI sequences were first extracted from the annotated plasmid sequences, and their secondary structures were predicted using the RNAfold Webserver (http://rna.tbi.univie.ac.at//cgi-bin/RNAWebSuite/RNAfold.cgi). **b)** The boxplots show the PCN of two replicons when they are found individually in different cells ("Single_2335", "Single_2358"), when they are co-integrated in the cell ("Multi-replicon") or co-residing as individual replicons within the same cell ("Single+Single") (Kruskal-Wallis test followed by Dunn's test for pairwise multiple comparisons, $p < 0.0094$), indicating that these two replicons were likely compatible and that their combined PCN was additive. **c)** The Venn diagrams show expected and observed counts for rep_2335, rep_2358, and genomes carrying co-existing single-replicon plasmids. Genomes bearing both single-replicon were overrepresented (Fisher's exact test $p < 10^{-12}$, odds ratio = 8.79), indicating that these two replicons are likely compatible.

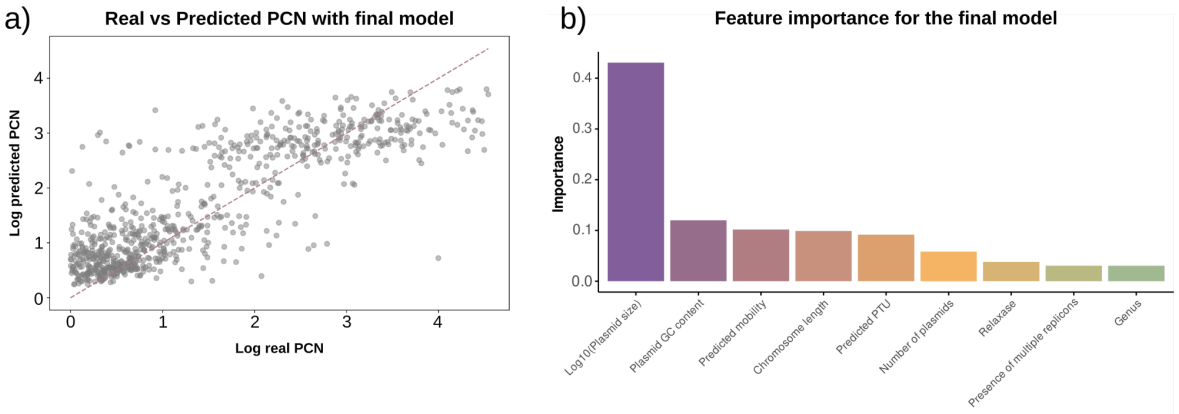

Extended Data Figure 15. Analysis of factors influencing plasmid copy number (PCN).

a) Performance of the Random Forest Regressor model in predicting PCN. The scatter plot shows predicted vs. observed PCN values. Each point represents an individual plasmid. **b)** Gini Feature importance plot from the Random Forest Regressor model. Bar height represents the relative importance of each variable for predicting PCN.

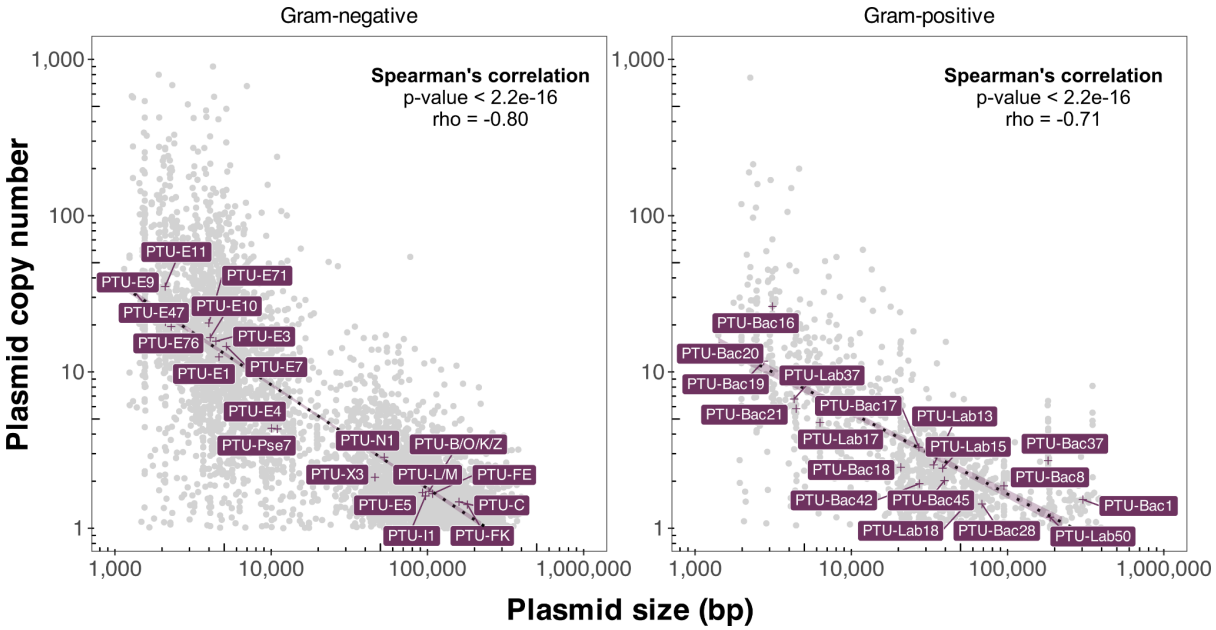

Extended Data Figure 16. The negative correlation between plasmid size and copy number is conserved.

Correlations between PCN (y-axis) and plasmid size (x-axis) for both Gram-positive and Gram-negative bacteria. Each dot represents a single plasmid, and the dotted line represents the best linear fit with 95% confidence intervals in light purple. The purple crosses and labels indicate each PTU's median PCN and size. Spearman's p-value and rho for correlations are also indicated within each plot (n= 5,181 for Gram-negative and n= 1,146 for Gram-positive).

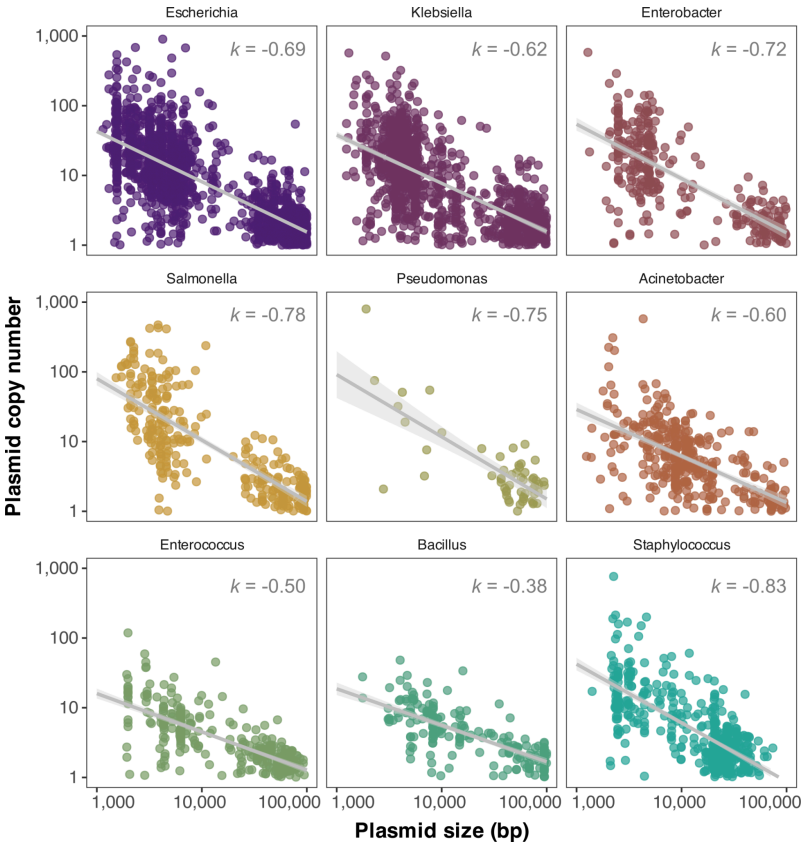

Extended Data Figure 17. Relationship between plasmid size and copy number across bacterial genera.

The scatter plots show the correlation between plasmid size (x-axis) and plasmid copy number (y-axis) for each genus. Each point represents an individual plasmid. The correlation is displayed by an ordinary least squares regression line (in gray), with the surrounding shaded area indicating the 95% confidence interval. The slope of the regression (*k*) is annotated at the top-right of each plot.

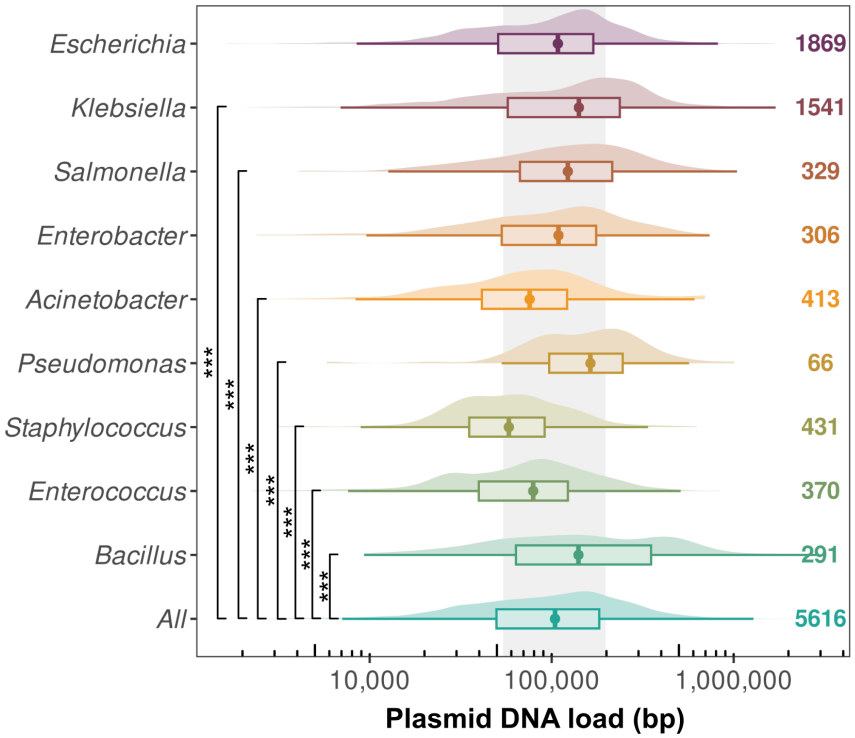

Extended Data Figure 18. Distribution of total plasmid DNA across different bacterial genera.

The y-axis represents the analyzed genera, while the x-axis represents the total DNA load per plasmid (bp), calculated as the product between PCN and plasmid size. The distributions (with boxplots overlaid) represent total plasmid DNA per genus (Kruskal-Wallis test followed by Dunn's test for pairwise multiple comparisons, p-value < 10^{-4}).

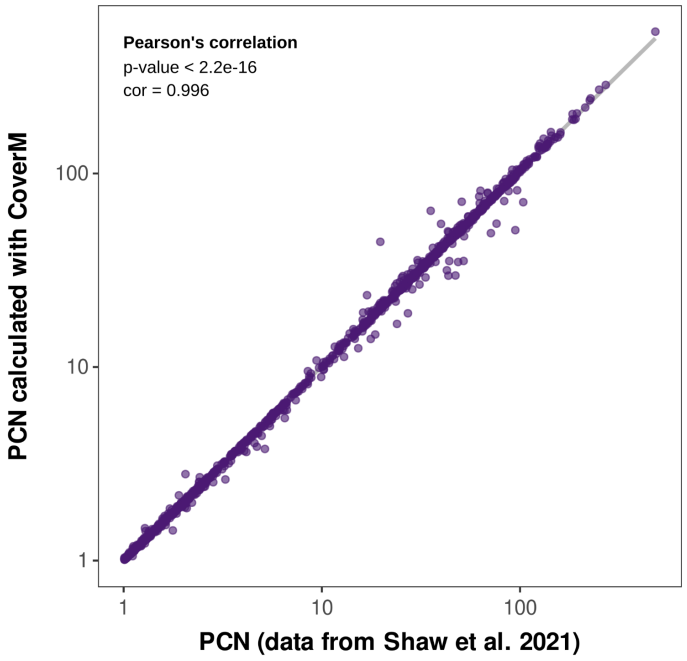

Extended Data Figure 19. Correlation of plasmid copy number estimates between methods. The x-axis represents PCN data calculated from Illumina sequencing from reference[17], and the y-axis represents PCN calculated using CoverM. Each point represents an individual plasmid. The gray line represents the line of best fit. Pearson's correlation coefficient (r = 0.996) and the associated p-value (< 10^{-16}) are shown in the top-left corner.

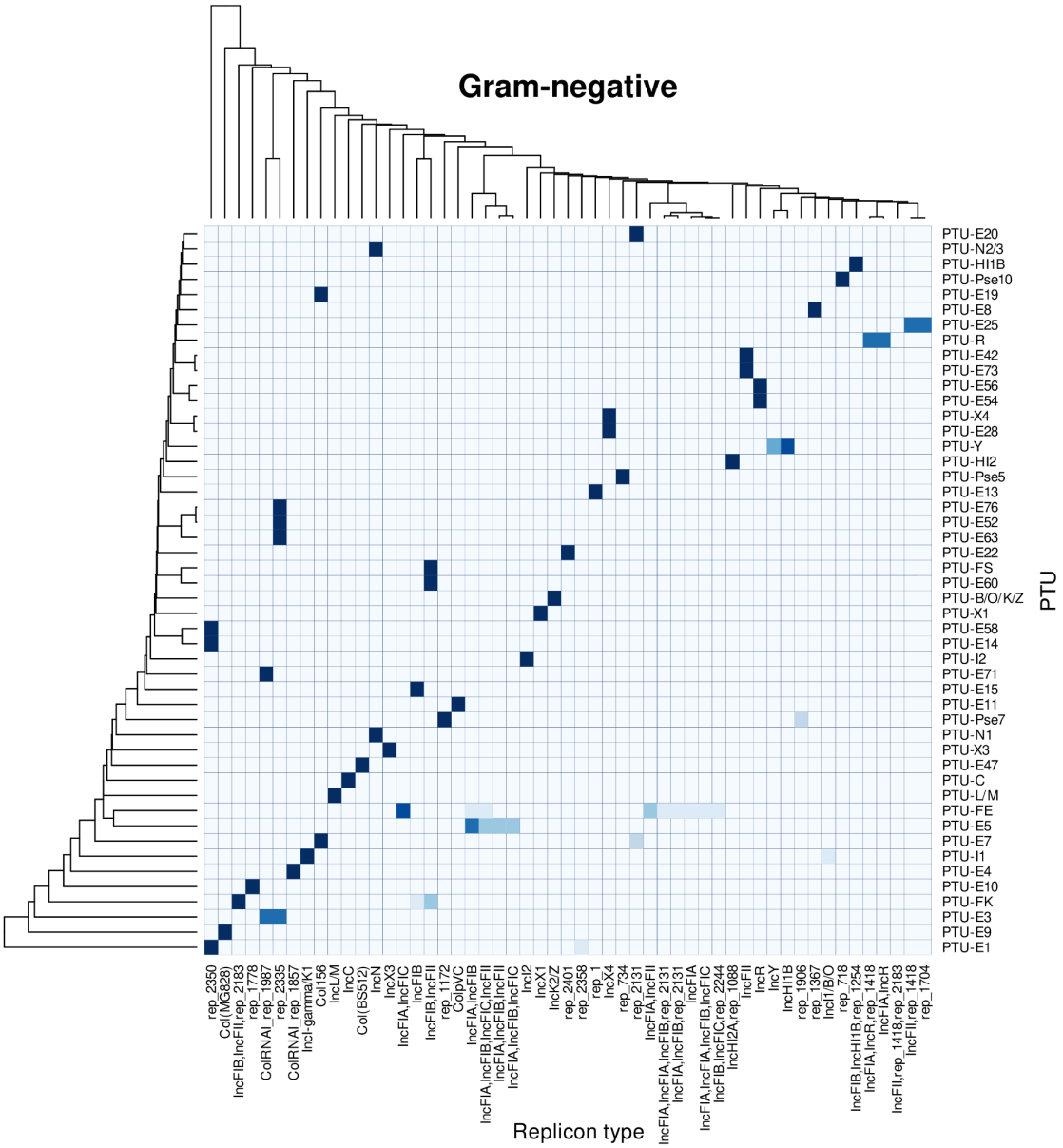

Extended Data Figure 20. Relation between PTUs and replicon types in Gram-negative hosts.

Heatmap displaying the association between PTUs (y-axis) and replicon types (x-axis) in Gram-negative bacteria. Based on their similarity, the dendrograms on the left and top of the heatmap show the hierarchical clustering of PTUs and replicon types. Each cell of the heatmap represents the strength of the association between a PTU and a replicon type. Darker shades of blue signify a stronger association, while lighter shades indicate weaker or no associations. Groups with an occurrence of <10 for Gram-negative and <5 for Gram-positive bacteria are not displayed.

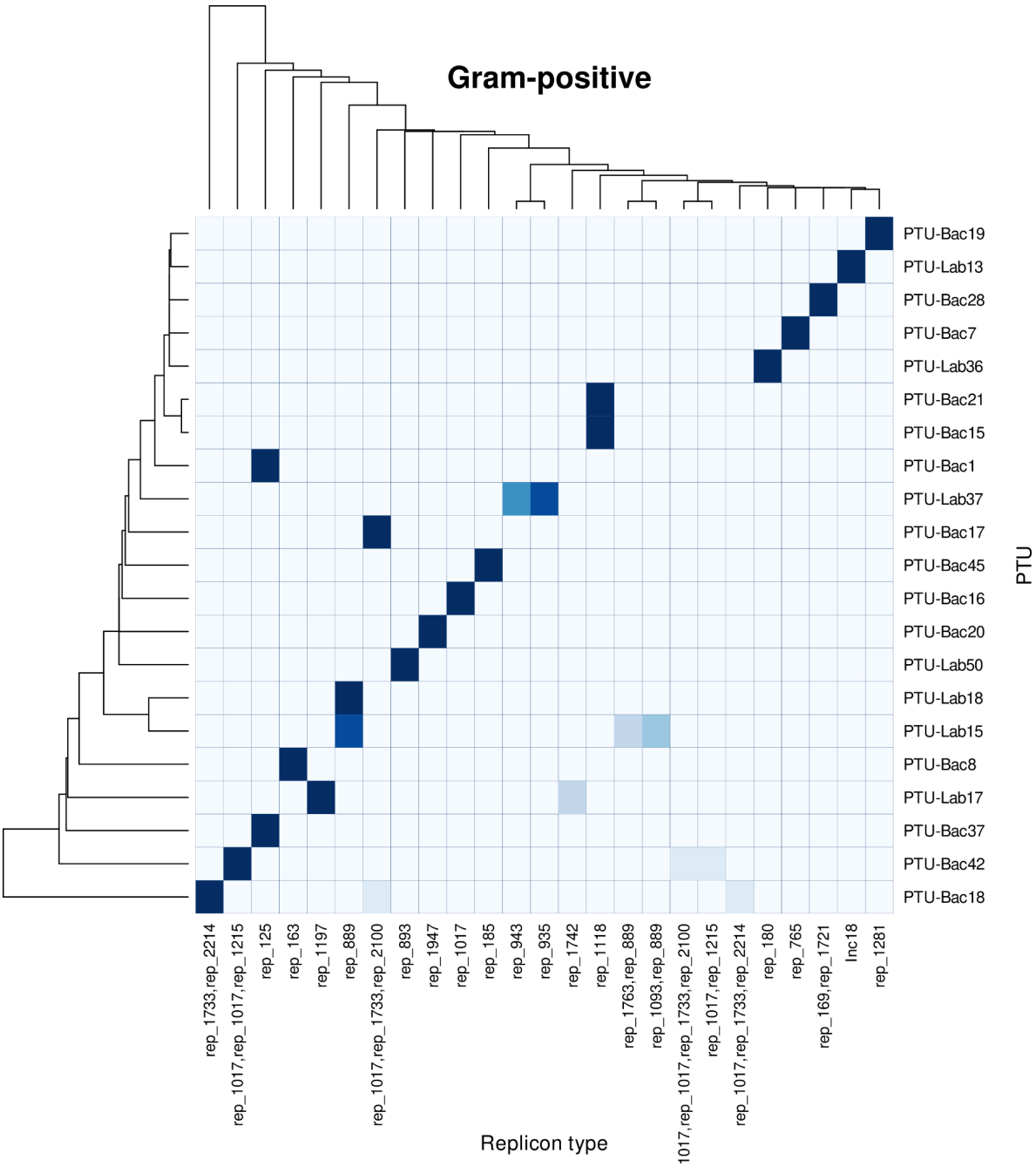

Extended Data Figure 20 (cont). Relation between PTUs and replicon types in Gram-positive hosts.

Heatmap displaying the association between PTUs (y-axis) and replicon types (x-axis) in Gram-positive bacteria. Based on their similarity, the dendrograms on the left and top of the heatmap show the hierarchical clustering of PTUs and replicon types. Each cell of the heatmap represents the strength of the association between a PTU and a replicon type. Darker shades of blue signify a stronger association, while lighter shades indicate weaker or no associations. Groups with an occurrence of less than <10 for Gram-negative and <5 for Gram-positive bacteria are not displayed.